The Solar Wind

M. Neugebauer and R. von Steiger

Parker's Theory and the Early Measurements of the Solar wind

Shortly before the beginning of the space age, Eugene N. Parker of the University of Chicago predicted that interplanetary space would be filled with a plasma flowing rapidly outward from the Sun (Parker, 1958). The likelihood that the Sun ejects charged particles that cause auroral and magnetic activity on Earth was generally accepted by that time. The observation that the plasma tails of active comets always point almost radially away from the Sun led Ludwig Biermann (1951) to postulate that the solar corpuscular radiation is continuous, rather than intermittent. It was also known that the outer atmosphere of the Sun, the solar corona, was extremely hot, with a temperature exceeding a million degrees. In 1957, Sidney Chapman (1957) calculated that if the corona was in hydrostatic equilibrium, it must extend throughout the solar system and cool off to only ~2×10^5 K at the orbit of Earth. Parker (1958) put all these ideas together, explaining that the inward pressure of the interstellar medium was too weak to allow the solar atmosphere to be in hydrostatic equilibrium. He coined the phrase "solar wind" to describe the outward flowing solar corona which supplies the

pressure required to stand off the local interstellar medium, to exert the necessary force on cometary plasma tails, and to transmit solar disturbances to the geomagnetic field. For a more complete theoretical explanation of Parker's prediction of the solar wind, see his article in this book.

Parker's theoretical prediction was not uncontested, however. Most notably, Joseph Chamberlain (1960) proposed that rather than Parker's solar wind caused by the hydrodynamic outflow of the solar corona, there was merely a solar breeze, consisting of plasma thermally escaping from the corona. Many of the early space investigations were therefore attempts to determine whether interplanetary space was filled with Parker's supersonic 500 km s^{-1} solar wind or with Chamberlain's subsonic 10 km s^{-1} solar breeze. A summary of those early missions and experiments is given in Table 1.

Not surprisingly, the Soviets were the first in space with instruments capable of measuring the interplanetary plasma. Their "ion traps" were simple Faraday cups with an inner grid held at –200 V to repel interplanetary electrons and to prevent the escape of photoelectrons from the cup and an outer grid at a positive potential to define the minimum energy of the ions entering the cup. Lunik II was the most successful of four missions, determining that there was indeed a flux of ~2×10^{8} cm^{-2} s^{-1} of positive ions with energy/charge > 15 eV/charge (Gringauz, 1960). Because the speed of a proton with energy >15 eV is >53 km s^{-1}, the Lunik II measurements favored Parker's theory over Chamberlain's, but questions of the extent to which the

speed exceeded that limit, the direction of the flow, and its persistence were left unanswered.

With the Explorer 10 mission in 1961, a group from the Massachusetts Institute of Technology made the first American measurements of the solar wind (Bonetti, 1963). Their instrument was an advance over the Soviet ion traps in that it had an additional grid which carried a positive square-wave potential to allow measurement of the ion energy spectrum without confusion between the flux of ions entering the detector (an ac signal) and the flux of photoelectrons knocked out of the negative inner grid (approximately a dc signal). Before the spacecraft batteries died at a distance of ~34 Earth radii, the instrument measured an intermittent flux of ions from a direction within a 20° by 80° window which included the direction from the Sun. When the ions (assumed to be protons) were detected, their flux was in the range 1.0 - 2.5×10^{8} $cm^{-2}s^{-1}$, their speed was ~280 km s^{-1}, and their flow was supersonic, as predicted by Parker's theory. In retrospect, the ion fluxes detected by Explorer 10 were not in the solar wind proper, but downstream of the Earth's bow shock, in the flank of the magnetosheath.

A group at the NASA Ames Research Center attempted to measure the solar wind with instruments on Explorers 12 and 14 in 1961 and 1962 (Bader, 1962; Wolfe, 1965). These instruments were curved plate analyzers with a voltage applied perpendicular to the ions' direction of motion to bend their trajectories onto a detector. On Explorer 12 there was a problem that the field of view of the instrument did not include the solar direction, and on Explorer

14 there was a problem with contamination of the ion signal by solar ultraviolet radiation when the instrument did face the Sun. Furthermore, on both missions, the spacecraft trajectories were almost entirely downstream of the bow shock.

About the same time as the unsuccessful attempts by Bader and Wolfe at NASA-Ames, one of the authors (MN) and her colleague, Conway Snyder, flew solar wind detectors on four different missions. The first two of those spacecraft, Rangers 1 and 2, failed to get out of low-Earth orbit, while the third spacecraft, Mariner 1, went astray and was destroyed by ground command. Finally, after some hair-raising misadventures (Neugebauer, 1997), Mariner 2 was safely placed on a trajectory to Venus. The Mariner 2 instrument was a curved-plate analyzer which measured the ion current reaching a collector at each of ten voltages on the deflection electrodes. Mariner 2 obtained a spectrum of the solar wind every 3.7 minutes almost continuously for 113 days. There was no longer any doubt that Parker had been correct; the solar wind exists.

Although the ion spectra obtained by Mariner 2 were very crude by today's standards, with measurable currents in no more than five energy/charge channels at any time, a lot of information about the properties of the solar wind could be gleaned from the data (Neugebauer, 1966). The solar wind blew continuously from within a ten degree cone centered on the Sun. The wind was organized into low- and high-speed streams (velocities of ~350 and 700 km s^{-1}, respectively), each of about 7 day's duration. The speed-

versus-time profiles were steepened on the leading edges of the fast streams where the increased density indicated a snow-plow effect. The proton temperature varied directly with the speed. These features are illustrated in Figure 1, which is a plot of 3-hour averages of the solar wind speed and temperature over five 27-day rotations of the Sun. The pattern roughly repeated from one rotation to the next. On average, the ion flux and density varied inversely as the inverse square of heliocentric distance between 1.0 and 0.7 AU.

It was often possible to detect a second spectral peak which was interpreted as being caused by alpha-particles (helium nuclei) moving with approximately the same speed as the protons. This second peak could not, however, be fit to a model in which the alphas had the same temperature as the protons; instead, equal thermal speeds were indicated. The abundance of the alpha-particles relative to the protons was sometimes highly variable from day to day.

Parker predicted not only the existence of the solar wind, but also the configuration of the interplanetary magnetic field (Parker, 1958). Because of the very high electrical conductivity of the solar corona, the plasma and the magnetic field must move together. That is, the solar field is frozen into solar wind. But at the same time that the field is being dragged nearly radially into space by the solar wind, it is still tied to the rotating Sun, with the result that the interplanetary field should have a spiral pattern with an angle to the radial direction of ~45° near 1 AU. The predicted spiral pattern of the field could be

discerned in the data of the magnetometer on Mariner 2; this is illustrated in Figure 2, where each point represents a running average of five hourly averages. Although there is a great deal of scatter, the points are distributed in the quadrants predicted by the Parker spiral model. The properties of the fluctuations about the spiral direction continue to be studied intensively to reveal some of the fundamental processes occurring in the solar wind. A change in the direction of the interplanetary field from the first to the third quadrant in Figure 2, or the reverse, indicates a reversal of the polarity of the interplanetary field with the field sometimes pointing in toward and sometimes pointing out from the Sun. Week-long periods of persistent polarity were named magnetic sectors by Wilcox and Ness (1965)

Morphology

The solar wind has probably been blowing for at least the past 3×10^9 years with essentially the same strength, as can be estimated by comparing the flux of xenon ions in today's solar wind with that deduced from the xenon content of the lunar regolith (Geiss, 1973). Observations of comet tails reveal that the solar wind did not stop blowing even during the Maunder minimum, from about 1645 to 1715 when there were essentially no sunspots.

It thus seems the solar wind is a ubiquitous and continuous phenomenon, but it is not a structureless one. Its density, speed, temperature, ion charge states, elemental composition, and other properties all vary with time and position on time scales from minutes (or less, but knowledge of fast

fluctuations is limited by the typical time resolution of today's ion sensors) up to decades (or more, limited by the short duration of the space era). The large-scale structures of the solar wind are conveniently divided into recurrent or quasi-stationary streams and transient flows.

The discovery of a 27-day (the synodic period of solar rotation) modulation of cosmic rays by Forbush in 1938 was conclusively traced to dynamical phenomena in the interplanetary medium and related to recurring coronal "active regions" (in the terminology of those days) by Simpson in 1954 (cf. Simpson, 1998)). As shown in Figure 1, such recurrent structure was indeed found in interplanetary space in the form of alternating high- and low-speed streams, each lasting several days. The polarity of the interplanetary magnetic field tended to remain constant throughout each of the high-speed streams, with consecutive streams having opposite polarities. It is important to note that there is not a one-to-one correspondence between fast streams and magnetic sectors. There need not be a fast stream within every magnetic sector, and the position of a fast steam relative to its magnetic sector boundary does not remain fixed in interplanetary space. The leading edge of each fast stream, where the solar wind speed increases, is now commonly call a corotating interaction region (CIR). Such interaction regions are an inevitable consequence if streams of sufficiently different speeds are emitted from the Sun at the same heliographic latitude. The effect of solar rotation is to eventually ram fast solar wind into slower wind emitted from more westerly heliographic longitudes. Figure 3 shows an early sketch and a newer version

of this scenario. The newer version also shows how the CIR develops in interplanetary space to engulf the magnetic sector boundary.

As a general rule, two magnetized plasmas cannot intermix without the benefit of magnetic reconnection or others type of plasma instability. Therefore, the fast and the slow solar wind streams remain separated out to large heliographic distances. Discontinuities separating the two wind types were first studied by Belcher and Davis (Belcher, 1971) using Mariner 5 data. Burlaga (1974) introduced the term "stream interface" for this boundary which is characterized by a decrease in density by a factor of ~2, accompanied by a similar increase in kinetic temperature. Sometimes, in order to enhance the signal, these two signatures are conveniently combined into the specific entropy argument, $T/n^{1/2}$, where T is temperature and n is density. As the solar wind expands to 1 AU and beyond, the stream interaction becomes progressively more pronounced. The leading (slow) plasma becomes accelerated and the trailing (fast) plasma becomes decelerated, building up hydromagnetic stresses that ultimately lead to the development of a pair of interplanetary shocks, a forward shock at the leading edge of the CIR and a reverse shock at the trailing edge. These shocks normally do not develop within 1 AU of the Sun. They were first identified between 1 and 5 AU by Smith and Wolfe (1976) using data from Pioneer 10 and 11. It is these corotating shocks that cause the 27-day modulation of cosmic rays mentioned above.

In 1973, the Skylab mission obtained images of the solar corona in soft x-ray wavelengths. These images demonstrated that Simpson's "active regions" were in fact X-ray-dark regions, now called coronal holes, with lower-than-average density and temperature. (In modern usage, an active region is a group of sunspots with flare activity.) Krieger et al. (1973) showed that large coronal holes were the source of the quasi-stationary high-speed streams, thus confirming Simpson's conjecture. From the data from the Helios mission obtained between 0.3 and 1 AU, Rosenbauer et al. (1977) recognized that fast streams are really distinct from the slow solar wind in their kinetic properties as well as in their elemental and charge state composition, thus defining the quasi-stationary solar wind as a two-state phenomenon. Using data from the IMP spacecraft, Bame et al. (1977) quite accurately called the fast streams a 'structure-free state' of the solar wind. Large-area coronal holes exist in the solar atmosphere mainly during the declining to minimum phase of the solar activity cycle, when they are more or less centered around the poles, but often develop large extensions to lower latitudes which are the main sources of fast streams near the ecliptic plane. Thus the fast streams and the CIR structure they generate are typical of solar minimum and cause an increase in the average solar wind speed during that period, as first demonstrated in a survey of a good part of solar activity cycle 20 by Feldman et al. (1978a).

When propagating out to larger heliocentric distances, the solar-wind velocity structure behaves as if passed through a low-pass filter, as was

observed and modeled by Gosling et al. (1976) using data from the first radial line-up of Pioneer 10 with the Earth. The formation of forward-reverse shock pairs is accompanied by smoothing of the smaller speed structures present at 1 AU. Ultimately even the shocks disappear. A CIR's forward shock will eventually hit the reverse shock of the previous CIR – which might well be its own if there is only one CIR per solar rotation – and cancel into a tangential discontinuity. At large distances, CIRs are thus expected to coalesce into corotating merged interaction regions (CMIRs). These can produce successive increases and decreases of cosmic ray intensity over a period of several solar rotations, but generally little or no long-lasting or net modulation (Burlaga, 1985; McDonald, 1997). The lack of net modulation is due to the C(M)IRs being quite limited in their latitudinal extent.

Smith et al. (1978) observed that the magnetic sector structure seen by Pioneer 11 gradually disappeared with increasing heliographic latitude and was nearly unipolar at merely 16° north in February 1976, i.e. around the minimum phase of solar cycle 20. From observations of the solar magnetic field, it is possible to infer a heliomagnetic coordinate system with its equator coinciding with the heliospheric current sheet. If the solar wind speed is plotted versus heliomagnetic latitude, an orderly picture emerges; slow wind is observed in a ±20° equatorial belt, while outside that belt there is only fast wind. This can be visualized in the "ballerina skirt" picture originally proposed by Alfvén (1977) and visualized in Figure 4.

This general picture of the regions of fast and slow wind was confirmed impressively and extensively two solar cycles later by the Ulysses mission (Wenzel, 1992) on its first polar orbit around the Sun, in 1992-98. Figure 5 is a polar plot showing fast streams in the polar regions bounding a band of slow wind between them, separated by remarkably sharp boundaries. This once again emphasizes the two-state property of the quasi-stationary solar wind. The sources of the two stream types, polar coronal holes for the fast streams and coronal streamers for the slow wind, can easily be seen on the superposed pictures of the solar disk and corona. Note the strong superradial expansion of the fast streams which reach down to ~ ±20° latitude whereas the boundaries of the coronal holes lie near ±60°.

Long before the existence of the solar wind was established, it was known that times of high solar activity (sunspot number), recurring every 11 years, coincided with high geomagnetic activity, as conjectured by Lord Carrington in the 1850s and established by Birkeland around the turn of the century. Since CIRs are recurrent and characteristic of the minimum heliosphere, a different interplanetary structure must account for those geomagnetic disturbances, which are transient and characteristic of maximum activity. An obvious candidate is solar flares, which occur in solar active regions (sunspot groups) and were thought to eject streams of plasma into interplanetary space (Chapman, 1931) that in turn would disturb the geomagnetic field several days later.

It was not until the Skylab era, when the corona became observable for longer periods than just the few minutes of a total solar eclipse, that such events were indeed observed by a coronagraph (MacQueen, 1974), and the term coronal mass ejection (CME) was coined to describe them. Since then, thousands of CMEs have been observed with coronagraphs on Solwind, the Solar Maximum Mission (SMM), and the Solar Oscillation and Heliospheric Observatory (SOHO). An example from SMM is given in Figure 6. The picture shows the development of a particularly large CME in several steps. Initially, only an outer rope or bubble of enhanced density is visible. The loop then expands, and an apparent void – a region of low particle density and high magnetic field strength – appears within. Some CMEs also show an erupted prominence within the dark region. However, the relation between CMEs, erupting prominences, and solar flares is complex. Flares and erupting prominences are neither necessary nor sufficient conditions for a CME. Moreover, even when a flare appears in close connection with a CME, the start of the CME often precedes the flaring activity. This has led Gosling (1993) to attribute the central role in the chain of transient events leading from the Sun to near-Earth space to CMEs rather than to flares (which is not to say – despite the mildly polemic title of Gosling's paper – that flares are irrelevant).

The discovery of CME plasma in interplanetary space predates the discovery of their optical counterparts at the Sun. Whereas at declining to minimum solar activity the time profile of the solar wind speed is dominated

by recurrent fast streams, transient (non-recurrent) disturbances become more important or even dominant during solar maximum conditions. It is not, however, a trivial matter to identify CMEs in interplanetary space. Because of the wide range of velocities with which CMEs leave the Sun (<50 km s^{-1} to >1200 km s^{-1}), their interplanetary signatures may differ widely. Moreover, the observing spacecraft may encounter different parts of a CME depending on its relative position to the ejected material, adding to the variability of the observations. It is therefore not possible to define the interplanetary signature of CMEs unambiguously, but only to give a list of characteristics of which some, but rarely all, apply to an individual event.

- The most energetic CMEs drive shocks into the preceding solar wind, as sketched in Figure 7, much like fast streams from coronal holes do. Sheeley et al. (1985) find that only 2% of the shocks observed in 1979-82 (solar maximum 21) on Helios were clearly *not* associated with CMEs. The converse is not true, though, as numerous (slow) CMEs were not associated with shocks.
- It is usually quite simple to distinguish CME-associated shocks from CIR-driven shocks based on the kinetic temperature of the driving material. Both the proton temperature (Gosling, 1973) and the electron temperature (Montgomery, 1974) within a CME tend to be unusually low for a given solar wind speed. The cause is probably the expansion of the ejecta into a larger volume than they would otherwise occupy.

- CME ejecta often contain an anomalously high helium abundance (Hirshberg, 1972) which can easily reach twice the average solar wind value of n_α/n_p = 0.04-0.05 and may go up to 0.30 in extreme cases. The source of these enrichments, which often are very patchy, may be pockets of dynamically accumulated helium that were left behind in the corona due to insufficient Coulomb drag with the solar wind protons (Geiss, 1970a).
- Bidirectional streaming of suprathermal electrons is an important indicator of CMEs (Montgomery, 1974). It is clear from Figure 7 that both ends of the solar magnetic field lines carried out in the ejecta may be rooted in the corona, thus allowing heat flux carried by the electrons to flow either way around the loop. Gosling et al. (1992) surveyed more than a full solar cycle (1978–1990) of near-Earth bidirectional streaming events and found a variation of a factor of at least seven between solar maximum (72/y) and minimum (<12/y), again underlining the importance of CMEs structuring the heliosphere at solar maximum.
- In about one third of the CMEs observed near Earth, the magnetic field inside the ejecta region undergoes a smooth rotation in at least one component, accompanied by an increase of the field strength and a temperature decrease. The magnetic field in such events, called magnetic clouds, have the configuration of a twisted flux rope (Burlaga, 1981; Lepping, 1990).

- Finally, the relative abundances and the charge states of heavy elements (carbon and heavier) are often significantly different within CME ejecta than in the surrounding solar wind. Charge states are generally higher, sometimes extremely so (Galvin, 1997). Henke et al. (1998) noted a correlation between CMEs with a magnetic cloud topology and high charge states. This signature makes it simple to distinguish (fast) CMEs from recurrent fast streams, in which the heavy ions invariably have relatively low charge states. In very rare cases, towards the end of a CME event, the charge states become extremely low, which may be interpreted as the passage of cool prominence material (Gloeckler, 1999).

Not all of these features that distinguish CMEs from the ambient, quasi-stationary solar wind apply to each event, which makes CMEs a highly variable class of events. These tell-tale properties are almost entirely based on observations near the ecliptic plane. To date, only a small number of CMEs have been observed outside the range of the equatorial streamer belt, and all of them were fully immersed in coronal hole-associated fast wind near solar minimum (Gosling, 1994a). The plasma in all those CMEs had approximately the speed of the ambient (fast) solar wind of ~750 km/s. Nevertheless, most of them were preceded by a forward shock and, unlike at low latitudes, followed by a reverse shock. The presence of a shock pair indicates that they were not generated by the CME overtaking the wind, but by its over-expansion into the ambient plasma, i.e., by the same process responsible for the low kinetic

temperatures within. Near solar maximum, high-latitude CMEs may look much like their low-latitude cousins if slow solar wind dominates at all latitudes, but only the polar passes of the Ulysses mission during the upcoming solar maximum in 2000 or 2001 will tell.

The high rate of CME occurrence around solar maximum has a strong effect on the outer heliosphere. CME-generated transient interaction regions coalesce and form merged interaction regions (MIRs), which may be so numerous and extended at solar activity maximum that they cover the full solid angle around the Sun to become a global MIR, or GMIR (McDonald, 1997). It is these GMIRs that are responsible for the attenuation of galactic cosmic ray fluxes during solar maximum. When a GMIR reaches the heliopause, it creates radio emission of about a year's duration, as discovered by Gurnett and Kurth (1996) on Voyager 1 both for cycles 21 and 22. From the travel times of these radio signals it is possible to estimate the overall size of the heliosphere, which these authors give as 110–160 AU.

Composition

Some of the motivation for studying the abundances of heavy ions in the solar wind is summarized in Figure 8. The protosolar nebula formed from the interstellar medium ~4.6×10^9 years ago. Its composition is best preserved in the outer convective zone (OCZ) of the Sun, which can be regarded as well mixed and unaffected by fractionation processes (with a few exceptions). In the meantime, the local interstellar medium (LISM) has evolved chemically

due to many generations of stars, and has been mixed continuously due to the 250×10^6 year galactic rotation. Differences in the compositions of the present OCZ and LISM can therefore be used to estimate the average evolution of the galaxy over the lifetime of the Sun (Geiss, 1998). Similarly, differences in the compositions of the OCZ and various planetary materials provide clues to the evolution of the solar system. Remote sensing can provide some elemental abundances of the OCZ (Grevesse, 1998), but most solar isotopic abundances are not yet known. The elemental and isotopic compositions of the solar wind are therefore highly relevant to understanding the evolution of the galaxy and the solar system. The solar wind, however, provides a biased sample of the OCZ because the mechanisms that generate the solar wind do not operate equally strongly on all elements. A fractionation is imposed that depends on elemental parameters such as ion mass, mass per charge ratio, first ionization potential, etc. The resulting fractionation can only be assessed and characterized by comparing in situ measurements of the solar wind with remote observations of the photosphere. But once the fractionation mechanisms are understood, the process can be reversed and solar wind measurements can be used to infer the OCZ composition by theoretical modeling.

The second motivation for studying heavy ions is that the abundances, charge states, and kinetic properties of these ions provide information about the processes of coronal heating and solar-wind acceleration. Heavy ions are ideal for this purpose because they act as tracers which have little effect on the

large-scale dynamics and because, as shown later, the different types of solar wind flow have different heavy-ion properties.

Solar wind composition instruments of increasing complexity, resolution, and dynamic range have been flown on many spacecraft. Three generations of sensors can be distinguished.

The first solar wind instruments were either Faraday cups combined with retarding potential grids or curved-plate analyzers. Such electrostatic analyzers measure the energy per charge, E/q, of the incident ions, where $E = mV^2/2$ is the kinetic energy, m is ion mass, V is speed, and q is charge. By stepping the analyzer through a series of (usually log-spaced) voltage steps, the distribution function (phase space density as a function of energy or velocity) of the ion beam is obtained. If all ions in the solar wind have approximately the same flow speed and if the velocity spreads due to thermal motions of the ions are small enough to avoid overlap of neighboring peaks, an E/q spectrum can be interpreted as a m/q spectrum. The very early solar wind measurements resolved helium from hydrogen in this way (Neugebauer, 1966). Later sensors with better E/q resolution were able to record the low charge states of O, Si, and Fe at times when the solar wind kinetic temperature was sufficiently low (Bame, 1975a). At high kinetic temperatures, however, the individual peaks could not be resolved because they overlapped each other. Moreover, the high charge states of C and O always remained hidden behind the large He peak.

The second generation of sensors, first used by Ogilvie and Wilkerson (1969) on Explorer 34, had a velocity selector (a Wien filter) added after the *E/q* analyzer. By stepping both the analyzer and the selector voltages, it was possible to obtain *V* and *m/q* of the incident ions independently. With the ICI sensor on ISEE-3 (Coplan, 1978), it was possible to verify the equal-velocity hypothesis and to find deviations therefrom, as well as to determine the abundances and the kinetic properties of ^{3}He, ^{4}He, O, Si, and Fe under most solar wind conditions. That experiment additionally measured Ne (Kunz, 1983), but other important elements such as C and Mg still remained hidden due to *m/q* overlap with more abundant species. A different type of second-generation instrument consisted of an *E/q* analyzer with an array of solid state energy detectors (SSD) added, such as the ULECA instrument on ISEE-3 (Hovestadt, 1978). It was thereby possible to determine the charge states of the CNO group and Fe (Ipavich, 1986), but measurements were limited to high-speed solar wind due to the inefficiency of the SSD at low energy.

The third generation of instruments uses the time-of-flight (ToF) technique (Gloeckler, 1990). These sensors, of which SWICS on Ulysses is the first one to be flown in interplanetary space (Gloeckler, 1992), combine a classical *E/q* analyzer with a ToF measurement giving *V*, and a total energy *E* measurement in a solid state detector. Together, the three measurements provide energy (or speed), mass, and charge of each incoming ion separately. The main advantages of such an instrument are (1) a true mass measurement, thus resolving important *m/q* overlaps such as C^{6+}–He^{2+} or Mg^{10+}–C^{5+} and the

high charge states of Si and Fe, and (2) low background, due to the triple coincidence technique used in registering the start and stop pulses of the ToF path and the energy measurement. Because solid state detectors are inefficient at solar wind energies (~1 keV/amu), a post-acceleration of >~20 keV is needed to boost the ion energy. This also guarantees that solar wind of very different speeds is measured under nearly the same conditions inside the sensor. Comparisons of high-speed and low-speed solar wind composition can thus reliably be made. With SWICS/Ulysses, the abundances of C, N, Mg, and S were measured for the first time, as were the high charge states of O, Si, and Fe.

A different type of ToF sensor, such as SOHO/CELIAS/MTOF (Hovestadt, 1995), makes use of a harmonic retarding potential in which the time of flight is proportional to $\sqrt{m}$. These sensors reach a very high mass resolution of $m/\Delta m$ >~100 (at the expense of some detector efficiency and of the charge state information), allowing determination of elemental and isotopic abundances of several previously unmeasured elements such as Na, Al, and Ca (Bochsler, 1998).

A completely different type of solar wind sensor was carried on the Apollo missions (Geiss, 1970b). Thin Al and Pt foils were exposed to the solar wind on the lunar surface. A large, well-known fraction of the ions became trapped in the foils, which were returned for analysis by laboratory mass spectrometers. Noble gas abundances and highly accurate isotopic abundances could be obtained by this technique. It is planned to extend this

technique on NASA's Genesis mission in 2001. Finally, solar wind ions are also implanted in the lunar regolith, and solar-wind abundances, particularly the heavy noble gases Kr and Xe, can be obtained by analysis of the lunar material (Wieler, 1996).

An overview of a few selected solar wind parameters obtained by Ulysses over an 8-year period is given in Figure 9. The data were collected during the post-maximum phase of solar cycle 22 and the onset of cycle 23 and thus predominantly represent conditions of low solar activity. Two features are readily apparent from the figure. First, the bimodal property of the solar wind already noted in the bulk speed in Figure 5 is also apparent in the composition parameters. The Si/O ratio is clearly enhanced in the slow solar wind, as are the other elements (Fe, Mg) with a low first ionization potential (FIP). This is believed to be caused by FIP fractionation in the chromosphere (Geiss, 1982). The bimodality is even stronger in the charge state ratios, which are expressed here as equivalent temperatures for collisional equilibrium between ions and electrons. The conclusion is that the fast and slow winds originate in regions with different coronal temperatures. Second, all parameters are much more variable in the slow solar wind, which validates Bame's view (1977) of the fast solar wind as a structure-free state.

In 1993–94 and once again in 1996–97, slow wind alternated with a fast stream once every solar rotation (see Figure 9), yielding an ideal period for direct comparison of the two quasi-stationary stream types. Geiss et al. (1995a,b) performed a superposed epoch analysis of that period, with the

results shown in Figure 10. The figure summarizes in a compact way one of the most essential results of SWICS regarding solar wind composition. There are two quasi-stationary types of solar wind that differ in speed (a heliospheric signature), in charge state composition (a coronal signature), and in elemental composition (a chromospheric signature), and a sharp boundary separates the two states in the heliosphere, through the corona, and all the way down into the chromosphere. It is therefore quite likely that different physical processes must be invoked for the generation and acceleration of the two types of wind. From Figure 10 it is also apparent that the compositional jump is sharper at the leading side of the fast stream, i.e. within the CIR, than in the trailing rarefaction region. Wimmer-Schweingruber et al. (1997; 1999) have investigated exactly how sharp the jumps are and where they occur. Not surprisingly they identified the location of the change in composition with the stream interface, and they showed that the jumps in the charge state ratios usually occur faster than the time resolution of the sensor (~1 hour, depending on the particular ion species). The charge state ratio of O^{7+}/O^{6+} , for example is thus established as a powerful diagnostic tool for telling the two solar wind types apart. Such a tool is particularly useful for identifying cases of multiple stream interface crossings, or for telling fast quasi-stationary streams from fast CMEs.

The composition measurements are summarized in Figures 11 (elements) and 12 (charge states). The elemental data are plotted as the ratio of each element's abundance relative to oxygen observed in the solar wind to

the same ratio observed in the photosphere versus the first ionization potential. The difference between the fast and slow solar wind again stands out. It can also be seen in Figure 11 that elements with low FIP (<~10 eV) lie on a plateau a factor of ~3–5 above the elements with high FIP. The intermediate elements C and S with FIPs near 10 eV are also enriched in the solar wind, but by smaller factors. Up to Ne, the high-FIP elements also lie on a plateau, but He is under-abundant by a factor of ~2 relative to them. This basic FIP pattern was first described for the solar energetic particles by Hovestadt (1974), while Meyer (1981) first noted the same pattern in the slow solar wind near the ecliptic plane. In the fast streams, the fractionation factor between low- and high-FIP elements is reduced to a factor of ~2, but is still clearly present. Recent reanalysis of the Ulysses/SWICS data (von Steiger et al., 2000) indicate that the FIP bias of the slow wind is near the low end of the cited range, yet still significantly higher than in fast streams.

The observed compositional signature of fast streams must be imposed by a mechanism operating on the first ionization potential of the elements. It is generally accepted that the FIP fractionation occurs by atom-ion separation at an altitude where the solar atmosphere is partially neutral, i.e. in the upper chromosphere and the lower transition region of the Sun (Geiss, 1982). A broad variety of models has been proposed to explain the FIP effect (cf. von Steiger, 1997; Hénoux, 1998). Each model can be characterized by the mode of ionization and by the mode of separation invoked. Most of the models take UV and EUV photons as the agent of ionization, but little consensus exists

about the mode of separation. Atom-ion separation across magnetic field lines seems a good possibility, but there are several different ideas regarding the driving force (gravity, a density gradient, wave pressure, etc.). The different strengths of the FIP fractionation in the fast wind and in the slow wind perhaps implies that more than a single mechanism is at work

Average charge state spectra of the two solar wind types are shown in Figure 12. An obvious trend is a shift toward higher charge states in the slow wind compared to fast streams. Considering Figure 9, this comes as no surprise for C and O, since that shift translates directly into a higher freezing-in temperature. The situation for the elements that are spread over many charge states is less simple, however. The distributions of the low-charge states of Si and Fe are quite similar for both flow types, but there is an excess of high charge states in the slow wind. Only the fast-stream charge-state distribution can be represented quite well by a single freezing-in temperature for each element (Geiss, 1995a).

The charge state distribution of an element in the solar wind freezes in at that altitude in the corona where the ionization/recombination time scale exceeds the expansion time scale of the flow (Hundhausen, 1972). In fast streams, all charge states of an element indicate approximately the same temperature; the freezing-in temperatures for C, O, Fe, and Si are 1.0, 1.2, 1.25, and 1.45 MK, respectively (Geiss, 1995a). Combination of these temperatures with ionization and recombination coefficients can yield a rough radial profile of electron temperatures in the corona. It is sufficient to assume

a monotonically decreasing density as a function of heliocentric distance to show that the electron temperature must have a maximum of about 1.5 MK at a distance of a few solar radii (Ko, 1997).

Plasma Properties

The previous sections dealt with the macroscopic properties of the solar wind, including its organization into high- and low-speed streams and magnetic sectors and its chemical composition. A closer look, however, reveals that the solar wind is not an equilibrium plasma that can be described by locally unique values of velocity and temperature. Neither the ion nor the electron distributions are well described by Maxwell-Boltzmann functions, and several different streaming velocities and temperatures often exist simultaneously. These non-equilibrium distributions lead to some fascinating questions about plasma instabilities and wave-particle interactions, many of which are not yet well understood.

Consider first the solar wind electrons. The range of temperatures of solar-wind electrons is less than that of the ions. This is shown in Figure 13, where one-year averages of the electron and proton temperatures observed by the Earth satellite Vela 4 are plotted versus solar wind speed. Early measurements by Vela 4 and by OGO 5 also showed that the electron distribution is anisotropic and provides an average net heat flux of $\sim 10^{-2}$ erg cm^{-2} s^{-1} along the magnetic field and outward from the Sun (Montgomery,

1968, 1972; Ogilvie, 1971). This is much lower than the heat conduction expected from classical collision-dominated thermal conductivity.

Later observations of solar-wind electrons with the IMP 6-8 and Helios 1-2 spacecraft revealed an even more complex picture. The electron distribution can be usefully classified as consisting of a "core" population of thermal electrons, a faster, hotter "halo" population with a density ~5% of the density of the core (Feldman, 1975; Pilipp, 1987a), and sometimes a narrower, higher-energy beam called a "strahl" (Rosenbauer, 1977). Each of these electron populations is anisotropic with higher temperatures parallel to the magnetic field than perpendicular to it. The heat conduction occurs through the drift of the strahl and halo populations relative to the bulk speed. The details of the distribution functions depend strongly on the solar wind stream structure, with the anisotropy being greatest and the strahl being most prominent in the fast wind from coronal holes and with collisions being most important in the slow, dense wind near the heliospheric current sheet (Feldman, 1978b; Pilipp, 1987b). Near the heliospheric current sheet, the heat flux sometimes disappears, which is taken as evidence that magnetic reconnection has occurred across the current sheet so that the plasma is no longer magnetically connected to the Sun. At other times, double strahls are observed, with one beam of suprathermal electrons moving out from the Sun along a magnetic field line and the other beam headed back toward the Sun (Gosling, 1987; Pilipp, 1987c). As discussed earlier, such events are

interpreted as evidence for transient flow with a closed magnetic configuration in which both ends of the magnetic field lines are rooted in the Sun.

The variation of the electron distributions with distance from the Sun R were enabled by observations with Mariner 10 (0.45-1 AU), Helios 1-2 (0.29- 1 AU), Voyager 2 (1.0-4.8 AU), and Ulysses (1.0-5.4 AU). The temperature of the electron core component is usually fit to a power law, with the exponent ranging widely, from $R^{-0.24}$ to $R^{-1.26}$; these results differ from both adiabatic expansion, for which the power law exponent would be –1.33, and dominance by Coulomb collisions with an exponent of –0.33. The Helios and Ulysses measurements together indicate that the electron heat flux drops off approximately as $R^{-3.0}$ between 0.3 and 5 AU (Scime, 1994).

The velocity distribution of the protons in the solar wind is also anisotropic, usually with higher temperatures along the magnetic field than perpendicular to it (Hundhausen, 1967). At 1 AU, the proton heat flux is typically two or three orders of magnitude less than the electron heat flux. By the time of the IMP 6 mission, the energy resolution of electrostatic analyzers had improved to the point that two separate proton streams with different velocities could be discerned (Feldman, 1973). Helios 1 brought the first three-dimensional measurements of the solar wind plasma, which enabled mapping the distribution functions parallel and perpendicular to the field. Figure 14 shows samples of some of the variety of proton distribution functions observed by Helios 2. The inner contours indicate that in the core of the distribution the temperature perpendicular to the field is usually greater

than the parallel temperature, but the reverse is true for the outer contours. The top and bottom diagrams in the center column are examples of the presence of secondary proton beams streaming along the magnetic field with higher speeds than the core of the proton distribution. The average velocity difference between the primary and secondary proton beams increases with increasing wind speed and with decreasing distance from the Sun (Marsch, 1982a). Radial gradients of the temperature of solar wind protons have been measured with Helios 1-2, Pioneers 10-11, Voyager 2, and Ulysses. Approximately adiabatic expansion, with $T \propto R^{-4/3}$, was found in the slow solar wind (Marsch, 1982a; Liu, 1995), but in other flow regimes the proton temperature falls off more slowly than adiabatically, with power-law exponents in the range –0.7 to –1.0 (Marsch, 1982a; Gazis, 1994; McComas et al., 2000). With the SWICS instrument on Ulysses which can separate the distributions of different ion species, it was discovered that both the protons and the heavy ions have high-energy tails, extending to at least 10 thermal widths above the bulk speed, and containing up to 1% of the ion density (Ogilvie, 1993). These approximately exponential-shaped tails are most prominent following the passage of interplanetary shocks.

It has already been mentioned that the Mariner 2 data indicated that the alpha particles in the solar wind were ~4 times hotter than the protons, but later observations showed further peculiarities of the alpha distributions relative to that of the protons. Starting with the data from the Vela 3 spacecraft, it became apparent that, despite their greater mass, the alphas

were, on the average, moving away from the Sun faster than the protons (Robbins, 1970; Neugebauer, 1981). The vector velocity difference between the alphas and the protons, $V_{\alpha p}$, is parallel to the magnetic field. In the dense, slow solar wind, occasional Coulomb collisions limit the velocity difference to values close to zero. In the high-speed wind at 0.3 AU, Helios found values of $V_{\alpha p} \geq 150$ km s^{-1}, approaching the Alfvén speed V_A (Marsch, 1982b). Helios, Voyager 2, and Ulysses data all indicate that both $V_{\alpha p}$ and $V_{\alpha p}/V_A$ decrease with decreasing speed and with increasing distance from the Sun (Neugebauer, 1996). To complicate matters further, the alpha particle distributions also sometimes exhibit two beams (Feldman, 1973; Asbridge, 1976). Some of the variety of proton and alpha beams is illustrated in the one-dimensional spectra plotted in Figure 15.

The rare ions heavier than the alpha particles, from carbon to iron, tend to obey rather simple rules with surprising accuracy: the heavy ions all flow with the same bulk speed as the alphas, $V_i = V_\alpha$, and they all have equal thermal speeds, i.e. their kinetic temperatures are proportional to their masses, $T_i = m_i T_\alpha/4$. Adherence to these rules is illustrated in Figure 16 which shows data obtained near 5 AU by Ulysses/SWICS. The bulk speeds are equal to a very high degree of accuracy (<~1%) in both the slow and the fast solar wind. Closer to the Sun, near 1 AU, measurements of Si and Fe with the ISEE/ICI the SOHO/CELIAS instruments showed those elements lagging behind He at the higher speeds (up to 600 km s^{-1}) (Schmid, 1987; Bochsler, 1989; Hefti,

1998). A possible interpretation is that the acceleration up to the He speed is completed somewhere between 1 and 5 AU. The equality of the thermal speeds shown in Figure 16 is obeyed much less accurately, but because there is no systematic trend with either mass or mass per charge they may be considered equal despite the scatter. Most measurements at 1 AU, from ISEE/ICI (Bochsler, 1985) through SOHO/CELIAS (Hefti, 1998), also show equal thermal speeds of the heavy ions. An important exception to the rule is that when the solar wind is very slow and rather dense, Coulomb collisions tend to equalize the temperatures rather than the thermal speeds (Bochsler, 1985).

Conformance with these rules under most solar wind conditions suggests a rather simple physical interpretation, although a fully satisfying model of the underlying mechanism has not yet been developed. There is some consensus that interactions of the ions with Alfvén waves travelling outward on the bulk solar wind accelerate all heavy ions, irrespective of their mass, to a maximum velocity $\boldsymbol{V_i \leq V_p + V_A}$ **b,** where **b** is a unit vector parallel to the magnetic field. At the same time the heavy ions scatter in velocity space on a sphere around $\boldsymbol{V_i}$ with radius V_A, thus causing equal thermal speeds. A model by Isenberg and Hollweg (1983) reproduces the temperature rule for heavy ions quite well, but fails for their relationship to protons.

When examined on a finer temporal scale than that of the stream structure, the solar wind shows continuous fluctuations in nearly all parameters. There are many types of variations, arising from many different

sources or processes, and exhibiting many different modes of propagation or evolution. Because these disturbances propagate at speeds well below the solar wind speed, instruments on spacecraft sense only one-dimensional cuts through what are usually three dimensional structures or waves being carried outward from the Sun with the solar-wind fluid.

Perhaps the simplest variations to understand are those caused by changes in the solar source of the wind. Neighboring streamlines or magnetic flux tubes may contain plasmas with slightly different speeds, densities, temperatures, elemental compositions, and magnetic field strengths and directions. The flux tubes with higher pressure than their neighbors expand until, as discovered with the instruments on Voyager, pressure balance structures are a common feature of the solar wind far from the Sun (Vellante, 1987). The boundaries between plasmas from different sources are often quite sharp; these structures, called tangential discontinuities, can pass a spacecraft in a matter of seconds.

More prevalent than pressure balance structures are waves, of which many different kinds have been observed in the solar wind — electromagnetic, magnetohydrodynamic (MHD), magnetosonic, and electrostatic. The first waves to be studied in any detail were the low frequency, transverse MHD waves called Alfvén waves. Alfvén waves can be thought of as propagating kinks in magnetic field lines. These waves were first detected in the Mariner 2 data (Unti, 1968), but a study based on Mariner 5 data by Belcher and Davis (1971) led to a more complete

characterization of their properties. These large-amplitude, non-sinusoidal waves dominate the microscale structure of the solar wind at least half the time. They propagate outward from the Sun with wavelengths in the range 10^3 to 5×10^6 km. They are most prominent in the fast solar wind and in the trailing edges of high-speed streams and have the greatest amplitude in interaction regions. The MHD equations which describe a magnetized plasma such as the solar wind have solutions corresponding to longitudinal magnetosonic waves as well as the transverse Alfvén waves. The magnetosonic waves are seldom observed (Belcher and Davis, 1971), however, because they are rapidly damped (Barnes, 1966).

There is another family of solutions of the magnetohydrodynamic equations that corresponds to sharp jumps. The non-propagating tangential discontinuities (TDs) mentioned above are one solution, while propagating rotational discontinuities (RDs), which are sometimes thought of as steepened Alfvén waves, are another. Both types are seen in the solar wind at a rate of ~1/hour (Siscoe, 1968; Burlaga, 1969). There is a long-standing controversy, which is not yet resolved, about whether TDs or RDs occur more frequently. Other discontinuous solutions of the MHD equations correspond to shocks. The concept of collisionless shocks was first suggested by Gold (1959) as an explanation for the sudden commencement of geomagnetic storms, and, using data from Mariner 2, Sonett et al. (1964) were the first to demonstrate their existence.

Many high frequency waves are present in the solar wind in addition to the Alfvén waves and MHD discontinuities. Figure 17 displays the phase velocity versus wave frequency of some of the plasma wave modes seen in the solar wind near 1 AU; for simplicity the figure is limited to waves propagating along the magnetic field. Whereas the MHD waves with frequencies below the ion cyclotron frequency (f_c^+) are studied through their effects on the ions and the magnetic field, the higher frequency plasma waves require different instrumentation. Rapidly varying magnetic fields are measured by the voltage induced in a coil wound around a high permeability core, while electric fields are measured by the voltage difference between the two ends of long dipole antennas (often tens of meters long). Starting in the late 1960s, plasma wave instruments have been flown on a large number of spacecraft, including OGO 3 and 5, Pioneer 8 and 9, IMP 6, 7, and 8, Helios 1 and 2, ISEE 1, 2, and 3, Voyagers 1 and 2, and Ulysses.

The interesting questions are: Where do all these different waves come from? What causes them? How do they evolve in the solar wind? How do they affect the physics of the solar wind?

Some of the waves and other disturbances are generated at the Sun, or in the solar corona, while others are generated in situ in the solar wind. The observation that the great majority of the Alfvénic waves propagate outward from the Sun is the basis for the argument that these waves must be generated closer to the Sun than the so-called critical point where the flow speed first exceeds the Alfvén speed at which the waves propagate. These waves are

perhaps a remnant of the processes that heat the corona and accelerate the wind. Other waves are created by either dynamic or kinetic effects in the interplanetary medium. Regions where dynamic interactions generate waves include stream-interaction regions and other shear zones where the plasma may be subject to the Kelvin-Helmholtz instability.

Another burgeoning area of theoretical space plasma physics is MHD turbulence. As early as 1968, Coleman (1968) pointed out that the slope of power spectra of magnetic fluctuations in the solar wind was similar to the slope expected for isotropic, homogeneous fluid turbulence, and suggested that similar processes may occur in the solar wind. In the MHD turbulence view of the solar wind, the low-frequency Alfvén waves which propagate outward from the Sun or which are generated at shear regions in interplanetary space interact nonlinearly with each other or with a small population of inward propagating waves to produce higher frequency waves. The process continues, with the wave energy cascading downward to shorter wavelengths (higher frequencies). Eventually, when the wavelength reaches the ion cyclotron radius, the wave energy is absorbed by resonant ion heating. One such model by Tu (1988) successfully predicts both the change of slope and the variation of the proton magnetic moment as functions of distance from the Sun; the agreement between Tu's model and Helios measurements of the proton magnetic moment is shown in Figure 18. There continue to be many such studies using data from the Pioneer, Voyager, Helios, and Ulysses which focus on distinguishing non-propagating structures from radially evolving

turbulence, taking the three dimensional expansion and dynamics of the solar wind into account.

Almost all the non-equilibrium distributions discussed above are either the cause of or are limited by kinetic effects and instabilities. In a nearly collisionless plasma like the solar wind, waves play a role similar to that played by collisions in ordinary fluids. The dynamics of the solar wind can result in unstable, non-equilibrium distributions, which in turn result in the generation of waves. The waves then interact with the ions or electrons to return them toward an equilibrium configuration. The net effect is that the free energy present as a result of multiple beams or other anomalies is transferred, via wave-particle interactions, to more stable, but hotter distributions. As the wind flows out through interplanetary space, this heating results in radial temperature profiles that are less steep than expected for adiabatic flow. Studies of these instabilities and wave-particle interactions comprise a very large subdiscipline within space physics; only a few examples can be mentioned here.

It was mentioned previously that the electron heat flux is much less than that expected from collisional processes alone. There have been theoretical investigations of several instabilities that might limit this heat flux. Ulysses measurements showed that the upper limit of the electron heat flux decreases with solar distance as R^{-3}, which supports the whistler (electromagnetic) heat-flux instability proposed by Gary et al. (1994). The Ulysses data also showed a rough anticorrelation of the electron heat flux

with the simultaneously measured plasma wave amplitude detected by the radio/plasma wave experiment (Scime, 1996). The whistler waves had more than enough power to scatter electrons out of the halo, which carries most of the heat flux.

Another broad category of non-equilibrium wave-particle interactions involves ion beams, such as interstellar pickup ions or the streaming of a secondary beam of protons or a beam of heavy ions relative to the main proton fluid. Observations close to the Sun by the Helios spacecraft indicated that both the differential streaming between the primary and secondary proton beams and between the protons and alphas increase or decrease with increases or decreases in the Alfvén speed (Marsch, 1982a,b); although Alfvén waves must play a role in either accelerating or limiting the speed of the secondary beam, the details of the interactions are still an area of active investigation. Farther from the Sun, beyond 1 AU, where the relative velocities of the several beams become substantially less than the Alfvén speed, other processes must be at work. Knowledge of the generation of waves by and the pitch-angle scattering of pickup ions in the solar wind was greatly advanced by measurements of waves and particle distributions in the outer comas of comet Halley and other comets where the solar wind picked up freshly ionized cometary ions (Tsurutani, 1991).

The limitation of ion anisotropy is yet another example of important wave-particle interactions. In a nearly collisionless plasma such as the solar wind, one might expect an ion's magnetic moment (proportional to $T_\perp/B$) to

be conserved, which would imply that as the solar wind expands and the magnetic field becomes weaker, the velocity component perpendicular to the field would rapidly decrease to yield a ratio of $T_{\|}/T_{\perp}$ greatly in excess of the observed anisotropy. Using data from IMP 6, Bame et al. (1975b) showed, however, that in high-speed streams, the core of the proton distribution has $T_{\perp} > T_{\|}$, which the authors interpreted as the result of local, interplanetary heating.

Solar wind sources and acceleration mechanisms

Parker's original theory, which successfully predicted the existence of the solar wind, assumed a thermally driven, spherically symmetric, time stationary, nonmagnetic, single fluid. We have already seen that the solar wind consists of several fluids (electrons, protons, and heavy ions), each with their own temperatures and speeds, and often with multiple beams of a single particle type. The observed structure of fast, slow, and transient streams also tells us that the solar wind is neither spherically symmetric nor time stationary. It carries a magnetic field, which is too weak to affect the dynamics of the wind in interplanetary space, but which can control the motion of the plasma close to the Sun where the field is stronger. Finally, it turns out that the solar wind is not driven by thermal pressure gradients alone. This section provides a summary of the continuing effort to develop realistic models of the solar wind.

The early observations that the protons and electrons have different temperatures led to the development of two-fluid models of the solar wind (Sturrock, 1966). Use of two-fluid or multi-fluid models is justified by the low rate of Coulomb collisions between ions and electrons in interplanetary space. The two-fluid model predicted too high an electron temperature (3.4×10^5 K) and too low a proton temperature (4.4×10^3 K) at a solar distance of 1 AU. One must appeal to instabilities and wave-particle interactions to explain the redistribution of thermal energy from the electrons to the protons to provide the temperatures shown in Figure 13.

As mentioned earlier, it is well established that the fast wind emanates from coronal holes (Krieger, 1973). In coronal holes, the fields are obviously open, the expansion geometry appears to be simple, the acceleration occurs rapidly (Kohl, 1997), the charge states of heavy ions indicate a rapid freezing-in process, and the elemental abundances are close to solar values. On the other hand, bright features within coronal holes called polar plumes have been reported to have different elemental abundances than the fast solar wind. At least the prominently visible plume observed by Widing and Feldman (1992) appears to be enriched in low-FIP elements (such as in the Mg/Ne ratio) even more strongly than the slow solar wind. This is surprising because plumes are believed to be open-field structures within the coronal holes. It therefore seems that polar plumes are not a major source of the fast streams, and the absence of compositional variability in fast streams makes it questionable

whether plumes contribute to the solar wind at all. Plumes might be essentially static structures which don't participate in the outward mass flow; recent SOHO observations of flow speeds in plumes suggest that this might be the case (Giordano, 2000). Moreover, a systematic search for compositional fine structures as possible interplanetary remnants of polar plumes within the largely uniform fast streams, e.g. in microstreams or in pressure-balanced structures, has revealed only a possible small signature in charge states ratios, but no composition anomalies (von Steiger, 1997).

The single and multi-fluid models all result in solar wind speeds well below the values observed in flows emanating from coronal holes. As early as Mariner 2 it was clear that the fastest wind did not come from the hottest parts of the Sun (Snyder, 1966), as would be implied by a thermally driven model. In fact, the temperatures in coronal holes are lower than the temperatures of the rest of the corona. These facts led to a search for non-thermal methods of accelerating the solar wind. Leer and Holzer (1980) showed theoretically that the final state of the solar wind depends strongly on where energy or momentum is added to the flow. The observed high speeds can be achieved only if energy or momentum is added to the flow after it has reached supersonic speed; energy input at lower altitudes increases the density and the mass flux, but not the speed. One possible source of this additional energy or momentum is waves created close to the Sun that propagate out into the wind. The high flux of outward propagating Alfvén waves in the high-speed solar wind may be a remnant of such waves. The dependence of the differential

flow between the protons and the alphas (or heavier ions) on the Alfvén speed also suggests a role for Alfvén waves in the dynamics of the solar wind.

There may also be geometric effects on the acceleration of the solar wind. The polar coronal holes occupy only a small fraction of the solar surface, but the fast wind diverging from those holes occupies about 5 times the solid angle of the holes themselves. Wang and Sheeley (1990) derived an empirical relation between solar wind speed and the divergence of the coronal magnetic field in the region where the wind originates; fast wind comes from slowly diverging field lines and the slow wind can be mapped back to regions of highly diverging fields at the boundaries of coronal holes.

Another possibly important geometric effect is the lengthening of the path the electrons take from the Sun to the point of detection in the solar wind. The electron heat flux is not conducted radially away from the Sun, as assumed in some of the early models, but along the magnetic field lines. The spiral winding of the field due to the Sun's rotation slightly lengthens the path between the Sun and 1 AU, but the smaller scale twists, turns, and kinks in the field due to waves can lengthen the path considerably.

Probably all these effects — wave acceleration and heating, geometric effects, and a longer conduction path — play some role, but the entire process may be even more complicated than that. The heavy ion data demonstrate that it is not realistic to calculate the properties of the solar wind starting with some temperature and density at a given level in the corona. There are strong correlations between heavy-ion abundances (set in the chromosphere or

transition region), the ion charge states (set in the corona at distances of a few solar radii), and the speeds and temperatures of the heavy ions (probably set at altitudes where the wind has become supersonic). The three problems of how solar material is fed into the wind, how the corona is heated, and how the solar wind is accelerated are closely linked and must be solved together. This has not yet been done.

The energy required to heat the corona and to accelerate the wind must come from the turbulent convection in the outer layers of the Sun. The convection is thought to generate both waves which are damped in the chromosphere and corona and magnetic structures which relax by reconnection, but many questions remain about the nature of the waves and how they are damped and on the relative importance of magnetic reconnection. Some valuable information on coronal processes in the region of acceleration of the fast wind from coronal holes was obtained by SOHO. The Ultra-Violet Coronagraph Spectrograph (UVCS) instrument measures the intensities and profiles of the hydrogen Lyman α line and two lines of the O^{5+} ion in the corona from 1.5 to 5 solar radii (Kohl, 1995). The data provide information on the outflow velocities as well as on the random ("thermal") motions in both the solar radial and latitudinal directions. When combined with an empirical model of the coronal hole, the following results were obtained (Kohl, 1998): (1) The "thermal" velocities of the O^{5+} ions are much greater perpendicular to the magnetic field than parallel to it. (2) The

component of the "thermal" velocity perpendicular to the magnetic field is much greater for O^{5+} ions than for protons. (3) The outflow speed of O^{5+} ions is greater than the outflow speed of protons, which in turn is greater than that expected for electrons. These observations are inconsistent with any common motions of the O^{5+} ions and the protons; i.e., the "thermal" speeds cannot be due to transverse waves such as Alfvén waves or to turbulent motions. Kohl et al. (1998) suggest that the ion motions may be a signature of ion cyclotron waves. Lee and Wu (2000), on the other hand, believe that the proton and minor ion dynamics are signatures of fast shocks moving through the corona.

New questions arise. If these ion motions are a signature of ion-cyclotron waves, how are the waves generated? If they are shocks, what is the source of the shocks? McKenzie et al. (1995) suggest that waves are generated by "microflares" caused by magnetic reconnection at the boundaries of convection cells on the solar surface and that the heavier ions are preferentially heated by resonant dissipation of the resulting high-frequency ion-cyclotron waves. But there is currently no detailed theory or numerical model of how such microflares generate the spectrum of waves required to match both the SOHO UVCS observations in coronal holes and the properties of the solar wind ions from those holes observed in interplanetary space. Both the microflare model of McKenzie et al. and a model by Parker (1987; 1990) in which twisting of magnetic fields by turbulent motions of their footpoints on the solar surface to yield reconnection in "nanoflares" suppose the

acceleration and heating to occur in discrete bursts or jets rather than smoothly and continuously throughout the corona as a whole. Short-lived jets of material have, in fact, been observed to move up into the corona from the solar surface (Brueckner, 1983). Feldman et al. (1997) have proposed a composite model in which the bulk of the proton flux results from acceleration by thermal pressure gradients while discrete, transient jets contribute the higher speed secondary proton peak, the alpha particles, and the heavier ions.

Three sites have been suggested for the source(s) of the slow solar wind. Some of the slow wind can be traced back to small, low latitude coronal holes (Neugebauer, 1998). Some of it probably originates in the bright, dense coronal streamers like those shown in Figure 5 (Feldman, 1981). It is not clear, however, how the material escapes from the obviously closed magnetic structures at the base of the streamer. Two proposed explanations are (a) quasi-stationary reconnection at the top of the closed field lines near the base of the current sheet, or (b) flow from the roots of the streamer along the open field lines at its periphery. The two scenarios can be tested by examination of the composition of the slow solar wind, in particular around the times of current sheet crossings which are thought to map back to the tip of the closed field region. Oxygen is observed to have close to its normal abundance at times of sector boundary crossings (von Steiger, 1995). This clearly favors scenario (b) because SOHO/UVCS observations show that the abundances of oxygen and other high-FIP elements are depleted by an order of magnitude relative to photospheric values in the core of a quiescent equatorial streamer

but resemble abundances measured in the slow wind along its periphery (Raymond, 1997).

In all its parameters, the slow solar wind is more highly variable than the fast solar wind. Because this variability includes elemental abundances, the fluctuations must originate at the Sun. Time lapse sequences of coronagraph images acquired by the LASCO experiment on SOHO revealed discrete blobs of plasma which originate ~3-4 solar radii above the cusps of the closed helmet-shaped structures and which move radially outward as they accelerate up to speeds of 300 km s^{-1} near 25 solar radii (Sheeley, 1997).

How can this variability of the slow wind be explained? Fisk (1996) has proposed a new model of the interplanetary magnetic field to explain the latitudinal extent of the recurrent acceleration of energetic particles observed by Ulysses. In that model (Fisk, 1999), the open field lines at the edges of coronal holes continuously reconnect with neighboring closed field loops. When reconnection occurs, the plasma originally in the loop joins the slow solar wind, whose properties then vary according to the properties (such as size, density, and temperature) of sequentially opened loops. Within this framework, Schwadron et al. (1999) have suggested a way in which wave heating on coronal loops may explain both the stronger average FIP fractionation and the broader distribution of charge states (i.e., loop temperatures) in the slow solar wind compared to the fast wind.

Sequences of coronagraph images from Skylab (Gosling, 1974), Solwind (Howard, 1985), the Solar Maximum Mission (Hundhausen, 1988)

and SOHO (Howard, 1997) leave no doubt about the source of the transient solar wind; it is associated with the eruption of previously closed magnetic structures such as solar prominences. One type of such an event has been descriptively named "streamer blow-out". There is debate whether prominence eruptions cause CMEs or whether CMEs cause prominence eruptions (Hundhausen, 1988). There are several suggestions concerning the cause(s) of the sudden release of energy in coronal mass ejections; these include the emergence of additional magnetic flux from beneath the solar surface (Feynman, 1995) and the shear of previously emerged magnetic flux (Mikic, 1997).

Observations with the Ulysses spacecraft provided new insight into the interplanetary acceleration of the transient solar wind. When seen moving through the corona, most CMEs have speeds well below typical speeds of CMEs detected in the solar wind at 1 AU or beyond. Near Earth, CME speeds typically range from 350 to 500 km s^{-1}. However, every one of the six CMEs detected by Ulysses in the fast polar solar wind, at latitudes between 31°S and 61°S, had speeds greater than 650 km s^{-1} (Gosling, 1994b). The conclusion is that processes must be at work to accelerate the transient plasma up to approximately the speed of the ambient, quasi-stationary wind with which it interacts. Numerical models suggest a process in which a plug of slow CME plasma inserted into a fast wind is pushed on by the fast plasma behind it and will also be accelerated by the pressure gradient at its leading edge caused by

the plasma ahead running away from it (Gosling, 1996). Similar types of forces act to slow down fast CME material inserted into a slow ambient wind.

Future Directions

Since the early 1960s, solar wind studies have evolved from questioning the very existence and nature of the solar wind to seeking to understand some of the processes and mechanisms responsible for its properties.

- Perhaps the greatest unknown is the acceleration mechanism. For example, is the fast solar wind accelerated continuously by pressure gradients and waves or is it accelerated almost exclusively in discrete jets? For another example, what destabilizes large magnetic structures to yield CMEs? Addressing such questions probably requires sending a well instrumented spacecraft extremely close to the Sun, within a few solar radii of its surface.
- There is another large set of questions associated with wave-particle interactions and solar wind turbulence. Progress in these areas would benefit from multi-spacecraft observations with very high time resolution of variations of the ion and electron distribution functions.
- Although great progress has been made in characterizing the fractionation of heavy elements between the solar surface and the solar wind, this work is not quite sufficiently definitive to relate the composition of the solar wind to the average composition of the Sun's outer convective zone. Determination of the isotopic abundances of

the solar wind to an accuracy relevant to studies of solar system evolution (see Figure 8) must await the return of solar wind samples by the Genesis mission.

There are other challenging problems involving the solar wind in areas within the scope of other articles in this book. Of special interest to solar wind physicists are the acceleration of energetic particles in the solar wind and the interactions of the solar wind with planetary bodies and with the local interstellar medium.

Bibliography for Further Reading

A history of solar wind research, 1957 - 1970: Hufbauer, K, 1991. *Exploring the Sun*. Baltimore: Johns Hopkins Univ. Press. pp 213-258.

Broad overview of solar wind physics through the Helios missions: Schwenn, R, and Marsch, E, Editors, 1991. *Physics of the Inner Heliosphere, Vols 1 and 2*. Berlin: Springer Verlag.

Corotating interaction regions: Balogh, A, Gosling, J T, Jokipii, J R, Kallenbach, R, and Kunow, H, Editors, 1999. *Corotating Interaction Regions, Space Science Series of ISSI, Vol. 7.* Dordrecht: Kluwer Acad. Publ.

Coronal mass ejections: Crooker, N, Joselyn, J A, and Feynman, J, Editors, 1997. *Coronal Mass Ejections*. Washington: Amer. Geophys. Un.

Solar composition and heavy ions in the solar wind: Fröhlich, C, Huber, M C E, Solanki, S K, and von Steiger, R, Editors, 1998. *Solar Composition and its Evolution – from Core to Corona, Space Sciences Series of ISSI, Vol. 5.* Dordrecht: Kluwer Acad. Publ.

Most recent compendium of solar wind research: *Solar Wind Nine, Conf. Proc. 471.* Edited by Habbal, S R, Esser, R, Hollweg, J V, and Isenberg, P A. Woodbury, N.Y.: Amer. Inst. Phys.

References

Alfvén, H, 1977. Electric currents in cosmic plasmas. *Rev. Geophys., 15*, 271.

Asbridge, J R, Bame, S J, Feldman, W C, and Montgomery, M D, 1976. Helium and hydrogen velocity differences in the solar wind. *J. Geophys. Res., 81*, 2719.

Bader, M, 1962. Preliminary Explorer 12 data on protons below 20 keV. *J. Geophys. Res., 67*, 5007.

Bame, S J, Asbridge, J R, Feldman, W C, Montgomery, M D, and Kearney, P D, 1975a. Solar wind heavy ion abundances. *Solar Phys., 43*, 463.

Bame, S J, Asbridge, J R, Feldman, W C, Gary, S P, and Montgomery, M D, 1975b. Evidence for local ion heating in solar wind high speed streams. *Geophys. Res. Lett., 2*, 373.

Bame, S J, Asbridge, J R, Feldman, W C, and Gosling, J T, 1977. Evidence for a structure-free state at high solar wind speeds. *J. Geophys. Res., 82*, 1487.

Barnes, A, 1966. Collisionless damping of hydromagnetic waves. *Phys. fluids, 9*, 2427.

Belcher, J W, and Davis, L, Jr., 1971. Large-amplitude Alfvén waves in the interplanetary medium. *J. Geophys. Res., 76*, 3534.

Biermann, L, 1951. Kometenschweife und Solare Korpuskularstrahlung. *Zeit. Astrophys., 29*, 274.

Bochsler, P, Geiss, J, and Joos, R, 1985. Kinetic temperatures of heavy ions in the solar wind. *J. Geophys. Res., 90*, 10,779.

Bochsler, P, 1989. Velocity and abundance of silicon ions in the solar wind. *J. Geophys. Res., 94*, 2365.

Bochsler, P, 1998. Structure of the solar wind and compositional variations. *Space Sci. Rev., 85*, 291.

Bonetti, A, Bridge, H S, Lazarus, A J, Rossi, B, and Scherb, F, 1963. Explorer 10 plasma measurements. *J. Geophys. Res., 68*, 4017.

Brueckner, G E, and Bartoe, J-D F, 1983. Observations of high-energy jets in the corona above the quiet sun, the heating of the corona, and the acceleration of the solar wind. *Astrophys. J., 272*, 329.

Burlaga, L F, 1969. Directional discontinuities in the interplanetary magnetic field. *Solar Phys., 7*, 67.

Burlaga, L F, 1974. Interplanetary stream interfaces. *J. Geophys. Res., 79*, 3717.

Burlaga, L, Sittler, E, Mariani, F, and Schwenn, R, 1981. Magnetic loop behind an interplanetary shock: Voyager, Helios, and IMP 8 observations. *J. Geophys. Res., 86*, 6673.

Burlaga, L F, Pizzo, V, Lazarus, A, and Gazis, P, 1985. Stream dynamics between 1 AU and 2 AU: A comparison of observation and theory. *J. Geophys. Res., 90*, 7377.

Cane, H, 1997. The current status in our understanding of energetic particles, coronal mass ejections, and flares. In: *Coronal Mass Ejections, Geophysical Monograph, 99*. Edited by Crooker, N, Jocelyn, J A , and Feynman, J. Washington, D.C.: Amer. Geophys. Un. p. 205.

Chamberlain, J W, 1960. Interplanetary gas II. Expansion of a model solar corona. *Astrophys. J., 131*, 47.

Chapman, S, and Ferraro, V C A, 1931. A new theory of magnetic storms. *Terrest. Magnetism Atmos. Elect., 36*, 77.

Chapman, S, 1957. Notes on the solar corona and the terrestrial ionosphere. *Smithsonian Contrib. Astrophys., 2*, 1.

Coleman, P J, Jr., 1968. Turbulence, viscosity, and dissipation in the solar wind plasma. *Astrophys. J., 153*, 371.

Coplan, M A, Ogilvie, K W, Bochsler, P, and Geiss, J, 1978. Ion Composition Experiment. *IEEE Trans. Geosci. Electron., GE-16*, 185.

Dessler, A J, and Fejer, J A, 1963. Interpretation of K_p index and M-region geomagnetic storms. *Planet. Space Sci, 11*, 505.

Feldman, W C, Asbridge, J R, Bame, S J, and Montgomery, M D, 1973. Double ion streams in the solar wind. *J. Geophys. Res., 78*, 2017.

Feldman, W C, Asbridge, J R, Bame, S J, Montgomery, M D, and Gary, S P, 1975. Solar wind electrons. *J. Geophys. Res., 80*, 4181.

Feldman, W C, Asbridge, J R, Bame, S J, and Gosling, J T, 1978a. Long-term variations of selected solar wind properties: Imp 6, 7, and 8 results. *J. Geophys. Res., 83*, 2177.

Feldman, W C, Asbridge, J R, Bame, S J, Gosling, J T, and Lemons, D S, 1978b. Characteristic electron variations across simple high-speed solar wind streams. *J. Geophys. Res., 83*, 5285.

Feldman, W C, Asbridge, J R, Bame, S J, Fenimore, E E, and Gosling, J T, 1981. The solar origins of solar wind interstream flows: near-equatorial coronal streamers. *J. Geophys. Res., 86*, 5408.

Feldman, W C, Gosling, J T, McComas, D J, and Phillips, J L, 1993. Evidence for ion jets in the high-speed solar wind. *J. Geophys. Res, 98*, 5593.

Feldman, W C, Habbal, S R, Hoogeveen, G, and Wang, Y-M, 1997. Experimental constraints on pulsed and steady state models of the solar wind near the Sun. *J. Geophys. Res., 102*, 26,905.

Feynman, J, and Martin, S F, 1995. The initiation of coronal mass ejections by newly emerging magnetic flux. *J. Geophys. Res., 100*, 3355.

Fisk, L A, 1996. Motion of the footpoints of heliospheric magnetic field lines at the Sun: Implications for recurrent energetic particle events at high heliographic latitudes. *J. Geophys. Res., 101*, 15547.

Fisk, L A, Zurbuchen, T H, and Schwadron, N A, 1999. On the coronal magnetic field: Consequences of large-scale motions. *Astrophys. J., 521*, 868.

Galvin, A B, 1997. Minor ion composition in CME-related solar wind. In: *Coronal Mass Ejections, Geophysical Monograph 99*. Edited by Crooker, N, Joselyn, J A, and Feynman, J. Washington: Amer. Geophys. Un. p. 147.

Gary, S P, Scime, E E, Phillips, J L, and Feldman, W C, 1994. The whistler heat flux instability: Threshold conditions in the solar wind. *J. Geophys. Res., 99*, 23.

Gazis, P R, Barnes, A, Mihalov, J D, and Lazarus, A J, 1994. Solar wind velocity and temperature in the outer heliosphere. *J. Geophys. Res., 99*, 6561.

Geiss, J, Hirt, P, and Leutwyler, H, 1970a. On acceleration and motion of ions in corona and solar wind. *Solar Phys., 12*, 458.

Geiss, J, Eberhardt, P, Bühler, F, Meister, J, and Signer, P, 1970b. Apollo 11 and Apollo 12 solar wind composition experiments: Fluxes of He and Ne isotopes. *J. Geophys. Res., 75*. 5972.

Geiss, J, 1973. Solar wind composition and implications about the history of the solar system. *Proc. 13th Intl. Cosmic Ray Conf., 5*, 3375.

Geiss, J, 1982. Processes affecting abundances in the solar wind. *Space Sci. Rev., 33*, 201.

Geiss, J, Gloeckler, G, von Steiger, R, Balsiger, H, Fisk, L A, Galvin, A B, Ipavich, F M, Livi, S, McKenzie, J F, Ogilvie, K W, and Wilkin, B, 1995a. The southern high-speed stream: Results from the SWICS instrument on Ulysses. *Science, 268*, 1033.

Geiss, J, Gloeckler, G, and von Steiger, R, 1995b. Origin of the solar wind from composition data. *Space Sci. Rev., 72*, 49.

Geiss, J, and Gloeckler, G, 1998. Abundances of deuterium and helium-3 in the protosolar cloud. *Space Sci. Rev., 84*, 239.

Giordano, S, Antonucci, E, Noci, G, Romoli, R, and Kohl, J L, 2000. Identification of the coronal sources of the fast solar wind. *Astrophys. J., 531*, L79.

Gloeckler, G, 1990. Ion composition measurement techniques for space plasmas. *Rev. Sci. Instrum., 61*, 3613.

Gloeckler, G L, Geiss, J, Balsiger, H, Bedini, P, Cain, J C, Fischer, J, Fisk, L A, Galvin, A B, Gliem, F, Hamilton, D C, Hollweg, J V, Ipavich, F M, Joos, R, Livi, S, Lundgren, R, Mall, U, McKenzie, J F, Ogilvie, K W, Ottens, F, Rieck, W, 1992. The solar wind ion composition spectrometer. *Astron. Astrophys. Suppl., 92*, 267.

Gloeckler, G, Fisk, L A, Hefti, S, Schwadron, N A, Zurbuchen, T H, Ipavich, F M, Geiss, J, Bochlser, P, and Wimmer-Schweingruber, R F, 1999. Unusual composition of the solar wind in the 2-3 May 1998 CME observed with SWICS on ACE. *Geophys. Res. Lett., 26*, 157.

Gold, T, 1959. Plasma and magnetic fields in the solar system. *J. Geophys. Res., 64*, 1665.

Gosling, J T, Pizzo, V, and Bame, S J, 1973. Anomalously low proton temperatures in the solar wind following interplanetary shock waves -- Evidence for magnetic bottles? *J. Geophys. Res., 78*, 2001.

Gosling, J T, Hildner, E, MacQueen, R M, Poland, A I, and Ross, C L, 1974. Mass ejections from the sun: A view from Skylab. *J. Geophys. Res., 79*, 4581.

Gosling, J T, Hundhausen, A J, and Bame, S J, 1976. Solar wind stream evolution at large heliocentric distances: Experimental demonstration and the test of a model. *J. Geophys. Res., 81*, 2111.

Gosling, J T, Baker, D N, Bame, S J, Feldman, W C, Zwickl, R D, and Smith, E J, 1987. Bidirectional solar wind electron heat flux events. *J. Geophys. Res., 92*, 8519.

Gosling, J T, McComas, D J, Phillips, J L, and Bame, S J, 1992. Counterstreaming solar wind halo electron events: solar cycle variations. *J. Geophys. Res., 97*, 6531.

Gosling, J T, 1993. The solar flare myth. *J. Geophys. Res., 98*, 18,937.

Gosling, J T, McComas, D J, Phillips, J E, Weiss, L A, Pizzo, V J, Goldstein, B E, and Forsyth, R J, 1994a. A new class of forward-reverse shock pairs in the solar wind. *Geophys. Res. Lett., 21*, 2271.

Gosling, J T, Bame, S J, McComas, D J, Phillips, J L, Goldstein, B E, and Neugebauer, M, 1994b. The speeds of coronal mass ejections in the solar wind at mid heliographic latitudes: Ulysses. *Geophys. Res. Lett., 21*, 1109.

Gosling, J T, and Riley, P, 1996. The acceleration of slow coronal mass ejections in the high-speed solar wind. *Geophys. Res. Lett., 23*, 2867.

Grevesse, N, and Sauval, A J, 1998. Standard solar composition. *Space Sci. Rev., 85*, 161.

Gringauz, K I, Bezrukikh, V V, Ozerov, V D, and Rybchinskii, R E, 1960. A study of interplanetary ionized gas, energetic electrons, and solar corpuscular radiation using three-electrode charged particle traps on the second Soviet Cosmic Rocket. *Soviet Phys. : Doklady, 5*, 361.

Gurnett, D A, 1991. Waves and Instabilities. In: *Physics of the Innter Heliosphere. 2. Particles, Waves and Turbulence*. Edited by Schwenn, R, and Marsch, E. Berlin: Springer-Verlag. p. 135.

Gurnett, D A, and Kurth, W S, 1996. Radio emissions from the outer heliosphere. *Space Sci. Rev., 78*, 53.

Hefti, S, Grünwaldt, H, Ipavich, F M, Bochsler, P, Hovestadt, D, Aellig, M R, Hilchenbach, M, Kallenbach, R, Galvin, A B, Geiss, J, Gliem, F, Gloeckler, G, Klecker, B, Marsch, E, Möbius, E, Neugebauer, M, and Wurz, P, 1998. Kinetic properties of solar wind minor ions and protons measured with SOHO/CELIAS. *J. Geophys. Res., 103*, 29,697.

Henke, T, Woch, J, Mall, U, Livi, S, Wilken, B, Schwenn, R, Gloeckler, G, von Steiger, R, Forsyth, R J, and Balogh, A, 1998. Differences in the O^{7+}/O^{6+} ratio of magnetic cloud and non-cloud coronal mass ejections. *Geophys. Res. Lett., 25*, 3465.

Hénoux, J-C, 1998. FIP fractionation: Theory. *Space Sci. Rev., 85*, 215.

Hirshberg, J, Bame, S J, and Robbins, D E, 1972. Solar flares and solar wind helium enrichments: July 1965-July 1967. *Solar Phys., 23*, 467.

Hovestadt, D, 1974. Nuclear composition of solar cosmic rays. In: *Solar Wind Three*. Edited by C. T. Russell. Los Angles, CA: Univ. Calif. p. 2.

Hovestadt, D, Gloeckler, G, Fan, C Y, Fisk, L A, Ipavich, F M, Klecker, B, O'Gallagher, J J, Scholer, M, Arbinger, H, Cain, J, Hofner, H, Kunneth, E, Laeverenz, P, and Tums, E, 1978. The nuclear and ionic charge

distribution particle experiments on the ISEE-1 and ISEE-C spacecraft. *IEEE Trans. Geosci. Electron., GE-16*, 116.

Hovestadt, D, et al., 1995. Celias - Charge, Element, and Isotope Analysis System for SOHO. *Solar Phys., 162*, 441.

Howard, R A, N.R. Sheeley, J, Koomen, M J, and Michels, D J, 1985. Coronal mass ejections: 1979 - 1981. *J. Geophys. Res., 90*, 8173.

Howard, R A, Brueckner, G E, Cyr, O C S, Biesecker, D A, Dere, K P, Koomen, M J, Korendyke, C M, Lamy, P L, Llebaria, A, Bout, M V, Michels, D J, Moses, J D, Paswaters, S E, Plunkett, S P, Schwenn, R, Simnett, G M, Socker, D G, Tapin, S J, and Wang, D, 1997. Observations of CMEs from SOHO/LASCO. In: *Coronal Mass Ejections, Geophysical Monograph 99*. Edited by Crooker, N, Joselyn, J A, and Feynman, J. Washington: Amer. Geophys. Un. p. 17.

Hundhausen, A J, Bame, S J, and Ness, N F, 1967. Solar wind thermal anisotropies: Vela 3 and IMP 3. *J. Geophys. Res., 75*, 5265.

Hundhausen, A J, 1972. *Coronal Expansion and Solar Wind.* New York: Springer-Verlag.

Hundhausen, A J, 1988. The origin and propagation of coronal mass ejections. In: *Proc. of the Sixth International Solar Wind Conf., NCAR/TN-306+Proc*. Edited by Pizzo, V J, Holzer, T E, and Sime, D G. Boulder, CO: National Center for Atmospheric Research. p. 181.

Ipavich, F M, Galvin, A B, Gloeckler, G, Hovestadt, D, Bame, S J, Klecker, B, Scholer, M, Fisk, L A, and Fan, C Y, 1986. Solar wind Fe and CNO measurements in high-speed flows. *J. Geophys. Res., 91*, 4133.

Isenberg, P A, and Hollweg, J V, 1983. On the preferential acceleration and heating of the solar wind. *J. Geophys. Res., 88*, 3923.

Ko, Y-K, Fisk, L A, Geiss, J, Gloeckler, G, and Guhathakurta, M, 1997. An empirical study of the electron temperature and heavy ion velocities in the south polar coronal hole. *Solar Phys., 171*, 345.

Kohl, J L, et al., 1995. The ultraviolet coronagraph spectrometer for the Solar and Heliospheric Observatory. *Solar Phys., 162*, 313.

Kohl, J L, G.Noci, Antonucci, E, Tondello, G, Huber, M C E, Gardner, L D, Nicoloci, P, Strachan, L, Fineschi, S, Raymond, J C, Romoli, M, Spadaro, S, Panasyuk, A, Siegmund, O H W, Benna, C, Ciaravella, A. Cranmer, S R, Giordano, S, Karovska, M, Martin, R, 1997. First results from the SOHO ultraviolet coronagraph spectrometer. *Solar Phys., 175*, 613.

Kohl, J L, et al., 1998. UVCS/SOHO empirical determination of anisotropic velocity distributions in the solar corona. *Astrophys. J., 501*, L127.

Krieger, A S, Timothy, A F, and Roelof, E C, 1973. A coronal hole as the source of a high velocity solar wind stream. *Solar Phys., 29*, 505.

Kunz, S, Bochsler, P, Geiss, J, Ogilvie, K W, and Coplan, M A, 1983. Determination of solar wind elemental abundances from M/Q observations during three periods in 1980. *Solar Phys., 29*, 359.

Lee, L C, and Wu, B H, 2000. Heating and acceleration of protons and minor ions by fast shocks in the solar corona. *Astrophys. J.*, in press.

Leer, E, and Holzer, T E, 1980. Energy addition in the solar wind. *J. Geophys. Res., 85*, 4681.

Lepping, R P, Jones, J A, and Burlaga, L F, 1990. Magnetic field structure of interplanetary magnetic clouds at 1 AU. *J. Geophys. Res., 95*, 11,957.

Liu, S, Marsch, E, Livi, S, Woch, J, Wilken, B, von Steiger, R, and Gloeckler, G, 1995. Radial gradients of ion densities and temperatures derived from SWICS/Ulysses observations. *Geophys. Res. Lett., 22*, 2445.

MacQueen, R M, Eddy, J A, Gosling, J T, Hildner, E, Munro, R H, Newkirk, G A, Jr., Poland, A I, and Ross, C L, 1974. The outer solar corona as observed from Skylab: Preliminary results. *Astrophys. J., 187*, L85.

Marsch, E, Mühlhäuser, K-H, Schwenn, R, Rosenbauer, H, Pilipp, W, and Neubauer, F M, 1982a. Solar Wind Protons: Three-Dimensional Velocity Distributions and Derived Plasma Parameters Measured Between 0.3 and 1 AU. *J. Geophys. Res., 87*, 52.

Marsch, E, Mühlhaüser, K-H, Rosenbauer, H, Schwenn, R, and Neubauer, F M, 1982b. Solar wind helium ions: observations of the Helios solar probes between 0.3 and 1 AU. *J. Geophys. Res., 87*, 35.

McComas, D J, Bame, S J, Barraclough, B L, Feldman, W C, Funsten, H O, Gosling, J T, Riley, P, Skoug, R, Balogh, A, Forsyth, R, Goldstein, B E, and Neugebauer, M, 1998. Ulysses' return to the slow solar wind. *Geophys. Res. Lett., 25*, 1.

McComas, D J, Barraclough, B L, Funsten, H O, Gosling, J T, Santiago-Muñoz, E, Skoug, R M, Goldstein, B E, Neugebauer, M, Riley, P, and Balogh, A, 2000. Solar wind observations over Ulysses first full polar orbit. *J. Geophys. Res., 105*, in press.

McDonald, F B, and Burlaga, L F, 1997. Global merged interaction regions. In: *Cosmic Winds and the Heliosphere*. Edited by Jokipii, J R, Sonett, C P, and Giampapa, M S. Tucson, AZ: Univ. Ariz. Press. p. 581.

McKenzie, J F, Banaszkiewicz, B, and Axford, W I, 1995. Acceleration of the high speed solar wind. *Astron. Astrophys., 303*, L45.

Meyer, J-P, 1981. A tentative ordering of all available solar energetic particle abundance observations. *Proc. Int. Cosmic Ray Conf., 17(3)*, 145.

Mikic, Z, and Linker, J A, 1997. The initiation of coronal mass ejections by magnetic shear. In: *Coronal Mass Ejections, Geophysical Monograph 99*. Edited by Crooker, N, Joselyn, J A, and Feynman, J. Washington: Amer. Geophys. Un. p. 57.

Montgomery, M D, Bame, S J, and Hundhausen, A J, 1968. Solar wind electrons: Vela 4 measurements. *J. Geophys. Res., 73*, 4999.

Montgomery, M D, 1972. Average thermal characteristics of solar wind electrons, NASA SP-308. In: *Solar Wind*. Edited by Sonett, C P, Coleman, P J, Jr. and Wilcox, J M. Washington: National Aeronautics and Space Administration. p. 208.

Montgomery, M D, Asbridge, J R, Bame, S J, and Feldman, W C, 1974. Solar wind electron temperature depressions following some interplanetary

shock waves: Evidence for magnetic merging? *J. Geophys. Res., 79*, 3103.

Neugebauer, M, and Snyder, C W, 1966. Mariner 2 observations of the solar wind, 1: Average properties. *J. Geophys. Res, 71*, 4469.

Neugebauer, M, 1981. Observations of solar-wind helium. *Fund. of Cosmic Physics, 7*, 131.

Neugebauer, M, Goldstein, B E, Smith, E J, and Feldman, W C, 1996. Ulysses observations of differential alpha-proton streaming in the solar wind. *J. Geophys. Res., 101*, 17.

Neugebauer, M, 1997. Pioneers of space physics: A career in the solar wind. *J. Geophys. Res., 102*, 26887.

Neugebauer, M, Forsyth, R J, Galvin, A B, Harvey, K L, Hoeksema, J T, Lazarus, A J, Lepping, R P, Linker, J A, Mikic, Z, Steinberg, J T, von Steiger, R, Wang, Y-M, and Wimmer-Schweingruber, R F, 1998. The spatial structure of the solar wind and comparisons with solar data and models. *J. Geophys. Res., 103*, 14587.

Ogilvie, K W, and Wilkerson, T D, 1969. Helium abundance in the solar wind. *Solar Phys., 8*, 435.

Ogilvie, K W, Scudder, J D, and Sugiura, M, 1971. Electron energy flux in the solar wind. *J. Geophys. Res., 76*, 8165.

Ogilvie, K W, Geiss, J, Gloeckler, G, Berdichevsky, D, and Wilken, B, 1993. High-velocity tails on the velocity distribution of solar wind ions. *J. Geophys. Res., 98*, 3605.

Parker, E N, 1958. Dynamics of the interplanetary gas and magnetic fields. *Astrophys. J., 128*, 664.

Parker, E N, 1987. Magnetic reorientation and the spontaneous formation of tangential discontinuities in deformed magnetic fields. *Astrophys. J., 318*, 876.

Parker, E N, 1990. Intrinsic magnetic discontinuities and solar x-ray emission. *Geophys. Res. Lett., 17*, 2055.

Pilipp, W G, Miggenrieder, H, Montgomery, M D, Mühlhäuser, K-H, Rosenbauer, H, and Schwenn, R, 1987a. Characteristics of electron velocity distribution functions in the solar wind derived from the Helios plasma experiment. *J. Geophys. Res., 92*, 1075.

Pilipp, W G, Miggenrieder, H, Montgomery, M D, Mühlhaüser, K-H, Rosenbauer, H, and Schwenn, R, 1987b. Variations of electron distribution functions in the solar wind. *J. Geophys. Res., 92*, 1103.

Pilipp, W G, Miggenrieder, H, Montgomery, M D, Mühlhaüser, K-H, Rosenbauer, H, and Schwenn, R, 1987c. Unusual electron distribution functions in the solar wind derived from the Helios plasma experiment: Double-strahl distributions and distributions with an extremely anisotropic core. *J. Geophys. Res., 92*, 1093.

Raymond, J C, et al., 1997. Composition of coronal streamers from the SOHO ultraviolet coronagraph spectrometer. *Solar Phys., 175*, 645.

Robbins, D E, Hundhausen, A J, and Bame, S J, 1970. Helium in the solar wind. *J. Geophys. Res., 75*, 1178.

Rosenbauer, H, Schwenn, R, Marsch, E, Meyer, B, Miggenrieder, H, Montgomery, M D, Mühlhäuser, K H, Pilipp, W, Voges, W, and Zink, S M, 1977. A survey on initial results of the Helios plasma experiment. *J. Geophys., 42*, 561.

Schmid, J, Bochsler, P, and Geiss, J, 1987. Velocity of iron ions in the solar wind. *J. Geophys. Res., 92*, 9901.

Schwadron, N A, Fisk, L A, and Zurbuchen, T H, 1999. Elemental fractionation in the slow solar wind. *Astrophys. J., 521*, 859.

Schwenn, R, 1990. Large-scale structure of the interplanetary medium. In: *Physics of the Inner Heliosphere. 1. Large-Scale Phenomena.* Edited by R. Schwenn and E. Marsch. Berlin: Springer-Verlag. p. 99.

Scime, E E, Bame, S J, Feldman, W C, Gary, S P, Phillips, J L, and Balogh, A, 1994. Regulation of the solar wind electron heat flux from 1 to 5 AU: Ulysses observations. *J. Geophys. Res., 99*, 23401.

Scime, E E, Gary, S P, Phillips, J L, Balogh, A, and Lengyel-Frey, D, 1996. Electron energy transport in the solar wind: Ulysses observations. In: *Solar Wind 8*. Edited by Winterhalter, D, Gosling, J T, Habbal, S R, Kurth, W S, and Neugebauer, M. Woodbury, NY: Amer. Inst. Phys. p. 210.

Sheeley, N R, Jr., Howard, R A, Koomen, M J, Michels, D J, Schwenn, R, Mühlhäuser, K H, and Rosenbauer, H, 1985. Coronal mass ejections and interplanetary shocks. *J. Geophys. Res, 90*, 163.

Sheeley, N R, Jr., Wang, Y-M, Hawley, S H, Brueckner, G E, Dere, K P, Howard, R A, Koomen, M J, Korendyke, C M, Michels, D J, Paswaters, S E, Socker, D G, Cyr, O C S, Wang, D, Lamy, P L, Llebaria, A, Schwenn, R, Simnett, G M, Plunkett, S, and Biesecker, D A, 1997. Measurements of flow speeds in the corona between 2 and 30 R_S. *Astrophys. J., 484*, 472.

Simpson, J A, 1998. A brief history of recurrent solar modulation of the galactic cosmic rays (1937-1990). *Space Sci. Rev., 83*, 169.

Siscoe, G L, Davis, L, Jr., Coleman, P J, Jr., Smith, E J, and Jones, D E, 1968. Power spectra and discontinuities in the interplanetary magnetic field: Mariner 4. *J. Geophys. Res., 73*, 61.

Smith, E J, 1964. Interplanetary magnetic fields. In: *Space Physics*. Edited by LeGalley, D P, and Rosen, A. New York: J. Wiley & Sons, p. 350.

Smith, E J, and Wolfe, J H, 1976. Observations of interaction regions and corotating shocks between one and five AU; Pioneers 10 and 11. *Geophys. Res. Lett., 3*, 137.

Smith, E J, Tsurutani, B T, and Rosenberg, R L, 1978. Observations of the interplanetary sector structure up to heliographic latitudes of 16 degrees, Pioneer 11. *J. Geophys. Res., 83*, 717.

Snyder, C W, and Neugebauer, M, 1966. The relation of Mariner-2 plasma data to solar phenomena. In: *The Solar Wind*. Edited by R. J. Mackin and M. Neugebauer. New York: Pergamon Press. p. 25.

Sonett, C P, Colburn, D S, Davis, L, Jr., Smith, E J, and Coleman, P J, Jr., 1964. Evidence for a collisionfree magnetohydrodynamic shock in interplanetary space. *Phys. Rev. Lett., 13*, 153.

Sturrock, P A, and Hartle, R E, 1966. Two-fluid model of the solar wind. *Phys. Rev. Letters, 16*, 628.

Tsurutani, B T, 1991. Cometary plasma waves and instabilities. In: *Comets in the post-Halley era*. Edited by Newburn, R L, Jr., Neugebauer, M, and Rahe, J. Dordrecht: Kluwer Academic Publishers. p. 1171 .

Tu, C-Y, 1988. The damping of interplanetary Alfvénic fluctuations and the heating of the solar wind. *J. Geophys. Res., 93*, 7.

Unti, T W J, and Neugebauer, M, 1968. Alfvén waves in the solar wind. *Phys. Fluids, 11*, 563.

Vellante, M, and Lazarus, A J, 1987. An analysis of solar wind fluctuations between 1 and 10 AU. *J. Geophys. Res., 92*, 9893.

von Steiger, R, Wimmer-Schweingruber, R, Geiss, J, and Gloeckler, G, 1995. Abundance variations in the solar wind. *Adv. Space Res., 15(7)*, 3.

von Steiger, R, Geiss, J, and Gloeckler, G, 1997. Composition of the solar wind. In: *Cosmic Winds and the Heliosphere*. Edited by Jokipii, J R, Sonett, C P, and Giampapa, M S. Tucson: Univ. Ariz. Press. p. 581.

von Steiger, R, Schwadron, N A, Fisk, L A, Geiss, J, Gloeckler, G, Hefti, S, Wilken, B, Wimmer-Schweingruber, R F, and Zurbuchen, T H, 2000. Composition of quasi-stationary solar wind flows from SWICS/Ulysses. *J. Geophys. Res., 105*, in press.

Wang, Y-M, and Sheeley, N R, Jr., 1990. Solar wind speed and coronal flux-tube expansion. *Astrophys. J., 355*, 726.

Wenzel, K-P, Marsden, R G, Page, D E, and Smith, E J, 1992. The Ulysses Mission. *Astron. Astrophys. Suppl. Ser., 92*, 207.

Widing, K G, and Feldman, U, 1992. Elemental abundances and their variations in the upper solar atmosphere. In: *Solar Wind Seven*. Edited by Marsch, E, and Schwenn, R. Oxford: Pergamon Press. p. 405.

Wieler, R, Kehm, K, Hohenberg, C M, and Meshik, A P, 1996. Secular changes in the xenon and krypton abundances in the solar wind recorded in single lunar grains. *Nature, 384*, 46.

Wilcox, J M, and Ness, N F, 1965. Quasi-stationary corotating structure in the interplanetary medium. *J. Geophys. Res., 70*, 5793.

Wimmer-Schweingruber, R F, Bochsler, P, and Wurz, P, 1999. Isotopes in the solar wind: New results from ACE, SOHO, and Wind. In: *Solar Wind Nine. AIP Conf. Proc. 471*. Edited by Habbal, S R, Esser, R, Hollweg, J V, and Isenberg, P A. Woodbury, N.Y.: Amer. Inst. Phys. p. 147.

Wimmer-Schweingruber, R F, von Steiger, R, and Paerli, R, 1997. Solar wind stream interfaces in corotating interaction regions. *J. Geophys. Res., 102*, 17,407.

Wolfe, J H, and Silva, R W, 1965. Explorer 14 plasma probe observations during the October 7, 1962, geomagnetic disturbance. *J. Geophys. Res., 70*, 3575.

Table 1. The Earliest Attempts (1959-1962) to Observe the Solar Wind.

Date	Spacecraft	Institution	Instrument	Result
Jan. 2, 1959	Lunik 1	USSR	4 ion traps -10 to + 15 V	no publishable data
Sept. 12, 1959	Lunik 2	USSR	4 ion traps -10 to + 15 V	39 - 60 R_E flux > 15 eV ≈ $2x10^8$ $cm^{-2}s^{-1}$
Oct. 4, 1959	Lunik 3	USSR	4 ion traps -19 to + 25 V	one observation of flux > 20 eV ≈ $4x10^8$ $cm^{-2}s^{-1}$ other data < threshold (~10^8 $cm^{-2}s^{-1}$)
Feb. 12, 1961	Venus Probe	USSR	Ion traps 0 and 50 V	very intermittent data one observation of flux ≈ $4x10^8$ $cm^{-2}s^{-1}$
March 25, 1961	Explorer 10	MIT	Modulated FC	skimmed magnetopause flank consistent with flow from Sun measured n, V, T supersonic & superAlfvénic
Aug. 16, 1961	Explorer 12	NASA Ames	CPA	dayside magnetosheath didn't detect any ions
Aug. 22, 1961	Ranger 1	JPL	6 CPAs	failed to get out of parking orbit
Nov. 18, 1961	Ranger 2	JPL	6 CPAs	failed to get out of parking orbit
July 22, 1962	Mariner 1	JPL	CPA	destroyed by range safety
Aug. 27, 1962	Mariner 2	JPL	CPA	113 days of data continuous radial flow high, low speed streams *n, v, T* relations $v_\alpha \approx v_p$; n_α/n_p variable; $T_\alpha \approx 4\ T_p$
Oct. 2, 1962	Explorer 14	NASA Ames	CPA	mostly magnetosheath UV interference

FC is Faraday cup and CPA is curved plate analyzer.

Figure Captions

Figure 1. Three-hour averages of solar wind speed (bottom line) and proton temperature (top upper and lower limit bars) observed by Mariner 2 in 1962. From (Neugebauer, 1966).

Figure 2. Five-hour sliding averages of hourly averages of the radial (ΔB_Z) and in-ecliptic transverse (ΔB_Y) components of the interplanetary magnetic field measured by Mariner 2. The dashed line shows the expected relation for the Parker spiral. Figure from (Smith, 1964).

Figure 3. The first sketch of a CIR (left) is by Dessler and Fejer (1963). The authors realized that 'the collision of these plasmas will lead to the formation of two shock waves ...', but nevertheless they (or their draftsperson?) chose to extend the shock all the way back to the Sun. A more modern version (right) shows the complex CIR morphology, including how the magnetic sector boundary, well outside the high speed stream near the solar surface, will be engulfed into the CIR in interplanetary space. Figure from (Schwenn, 1990).

Figure 4. Sketch of the inner heliosphere during declining to minimum solar activity in terms of the "ballerina skirt" model proposed by Alfvén (1977). The coronal holes around each pole emit magnetically unipolar fast streams of

opposite polarity, between which the slow wind from the belt around the heliomagnetic equator is confined. The warp of the current sheet separating fields of opposite polarity makes it loosely resemble a ballerina's skirt. Figure from (Schwenn, 1990).

Figure 5. Bulk speed of the solar wind plotted versus heliographic latitude in a polar diagram. The color code indicates magnetic polarity; both fast streams are in fact magnetically unipolar, as brief reversals near the poles are spuriously caused by large-amplitude Alfvén waves. The fast steams occupy a much larger solid angle in the heliosphere than the coronal holes do on the Sun (visible on the inset image from SOHO/EIT), indicating a strong superradial expansion. The boundary between the stream types is very sharp, as seen in the left half of the figure obtained during Ulysses' fast latitude scan; it was crossed multiple times due to the warp of the "ballerina skirt" on the distant portion of the orbit (right half). Figure from (McComas, 1998).

Figure 6. Development of a large CME observed by the coronagraph on the Solar Maximum Mission. Figure from (Hundhausen, 1988). Figure courtesy of HAO/SMM C/P project team & NASA. HAO is a division of the National Center for Atmospheric Research, which is supported by the National Science Foundation.

Figure 7. Sketch of a CME in interplanetary space, consisting of a bubble of ejecta driving a shock into the preceding solar wind (which is only the case if the ejection speed is sufficiently high), with a sheath of compressed plasma and magnetic field in-between. Figure from (Cane, 1997).

Figure 8. Logic diagram showing the relation between galactic and solar system evolution and the solar wind.

Figure 9. Overview of selected solar wind parameters obtained on Ulysses. (top panel) Bulk speed of protons; (panels 2 and 3) C/O and Si/O abundance ratios; and (panels 4 and 5) freezing-in temperatures from the O^{7+}/O^{6+} and C^{6+}/C^{5+} charge state ratios. All parameters are plotted at a time resolution of 5 days. The bimodal property of the solar wind speed in Figure 5 can also be seen in some of the other parameters: A strong anticorrelation of the freezing-in temperatures with speed is obvious, as is an enhanced abundance of the low-FIP element silicon in the slow wind. The Ulysses orbit remained near the ecliptic plane from launch to Jupiter and was tilted by some 80° thereafter, diving through the ecliptic during the fast latitude scan in early 1995. Figure adapted from (von Steiger, 2000).

Figure 10. Superposed epoch plot of slow solar wind alternating with a fast stream once per solar rotation in 1992–93. The average profiles of the parameters in Figure 9 are superposed over nine recurrences of an average

duration of 26 days, and the data are repeated twice to emphasize the periodicity. The anticorrelation of the speed with the charge state temperatures and their positive correlation with the compositional signature, is evident. Note also that the jump is sharp at the leading (CIR) side of the fast stream, but extended over 4–5 days at the trailing (dwell) side. Figure after (Geiss, 1995).

Figure 11. Solar wind abundances of heavy ions relative to oxygen, X/O, related to the photospheric ratios, $(X/O)_{phot}$, as a function of first ionization potential. Figure adapted from (von Steiger, 1997).

Figure 12. Average charge-state spectra of C, O, Si, and Fe from SWICS/Ulysses, of fast and slow SW, respectively. Each spectrum was obtained from a long-term accumulation over ~600 days. Figure adapted from (von Steiger, 2000).

Figure 13. (Top) Dependence of electron and proton temperatures on the flow speed of the solar wind. (Bottom) The ratio of the electron to proton temperatures. Figure from (Montgomery, 1972).

Figure 14. Proton velocity distributions measured over a range of solar-wind speeds and solar distances by Helios 2. The two-dimensional plots are cuts through the 3-dimensionsl distributions in a plane defined by the velocity

vector (VX axis) and the magnetic field. Scales are in km s^{-1}. Continuous contour lines correspond to fractions 0.8, 0.6, 0.4, and 0.2 times the peak phase space density and dashed contours are logarithmically space to fractions of 0.1, 0.032, 0.01, 0.0032, and 0.001. Figure from (Marsch, 1982).

Figure 15. Radially projected count-rate spectra showing protons and alpha-particles in the trailing region of a high-speed stream. V_1 is the speed of the primary proton peak, V_A is the Alfvén speed, and V_2 is the speed of a secondary proton peak. Figure from (Feldman, 1993).

Figure 16. Bulk speeds (full symbols) and thermal speeds (open symbols) of heavy solar wind ions obtained with SWICS/Ulysses during two 5-day time periods in fast (circles, days 1-5 of 1994) and in slow (diamonds , days 1-5 of 1998) solar wind.

Figure 17. Plots of phase velocity versus frequency for selected plasma wave modes that propagate parallel to the interplanetary magnetic field. Figure from (Gurnett, 1991).

Figure 18. Plot of the proton magnetic moment $T_\perp/B$ as a function of solar distance. Figure from (Tu, 1988).

Fig 1
Neugebauer & von Steiger

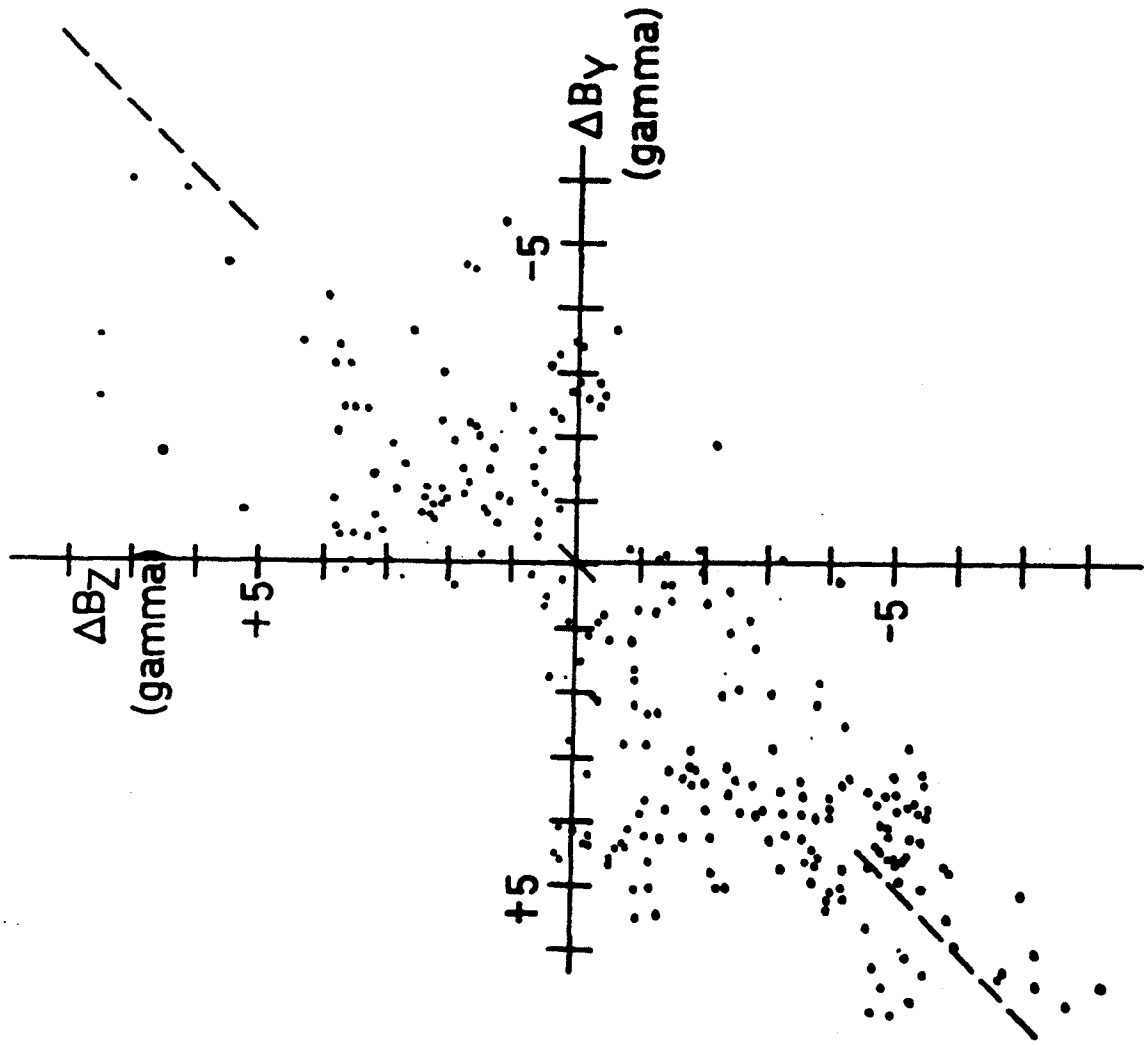

Fig 2

Neugebauer von Steiger

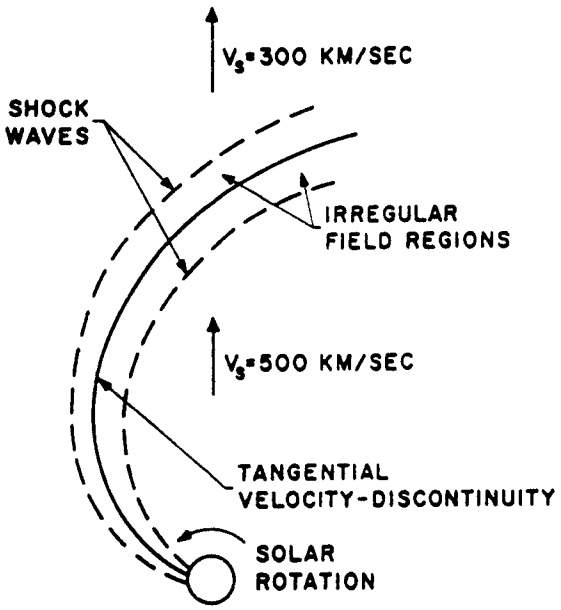

Fig 3-left

Neugebauer + von Steiger

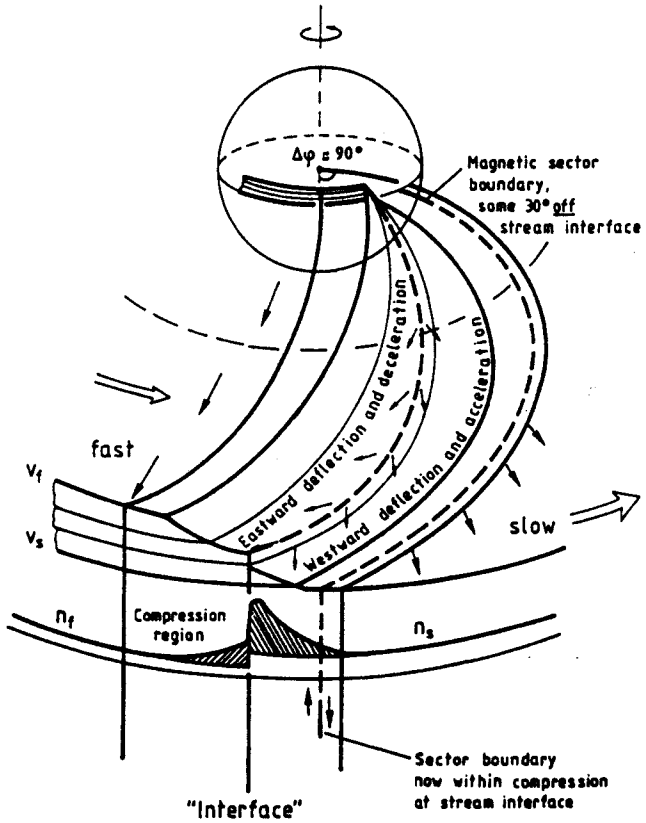

Fig 3 - Right

Neugebauer + von Steiger

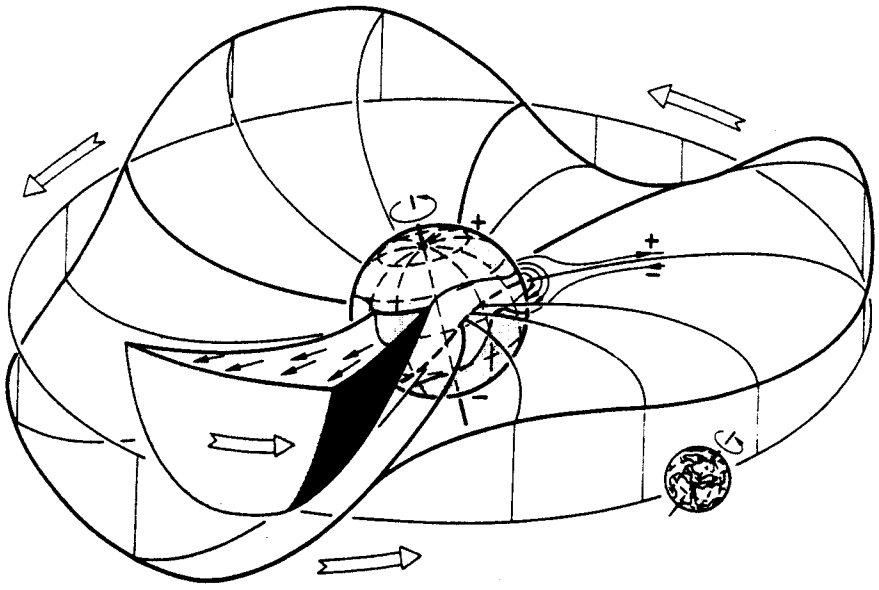

Fig 4

Neugebauer + von Steiger

Fig 5
Neugebauer von Steiger
Cubo

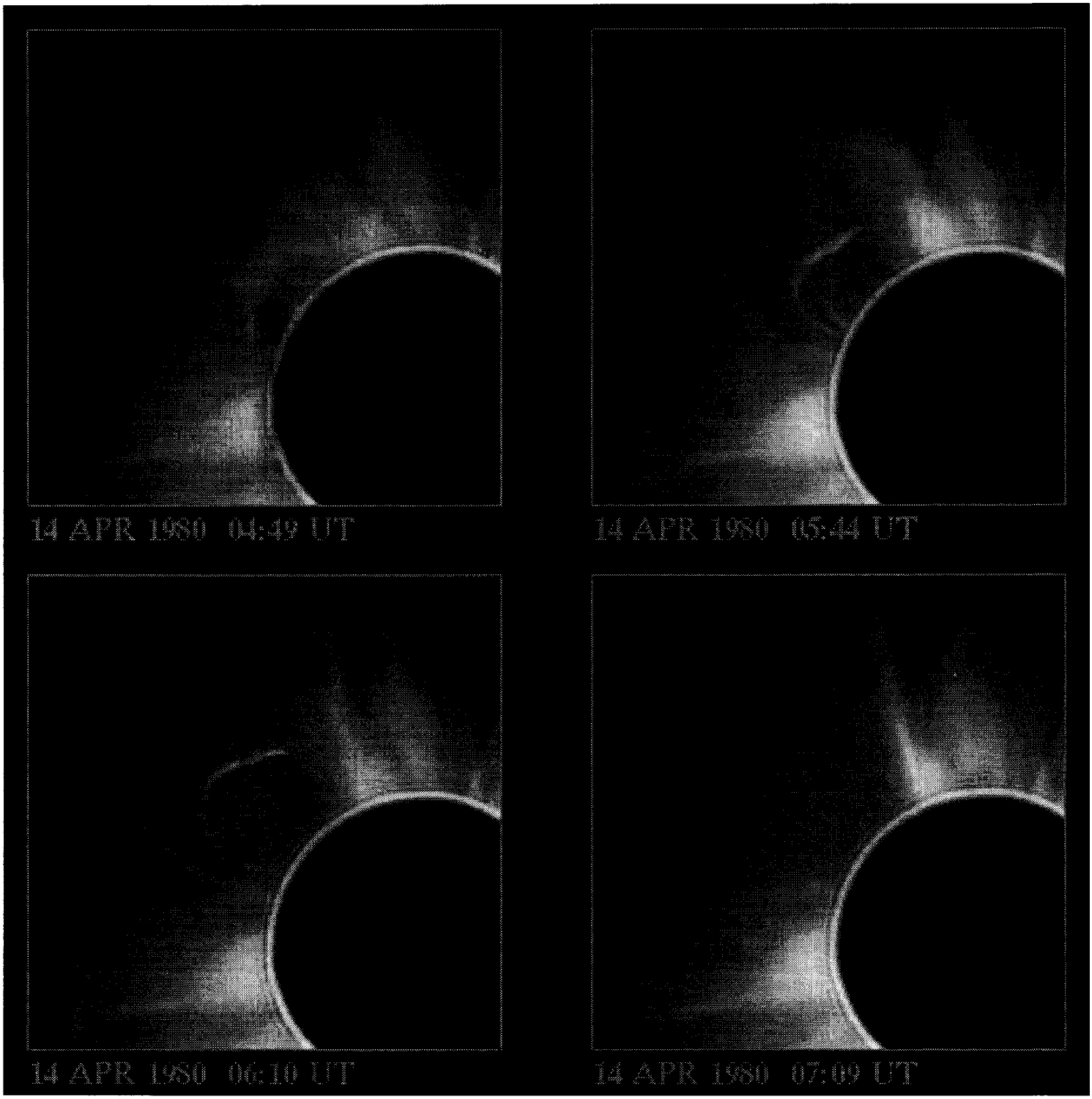

Fig 6
Neugebauer & von Steiger

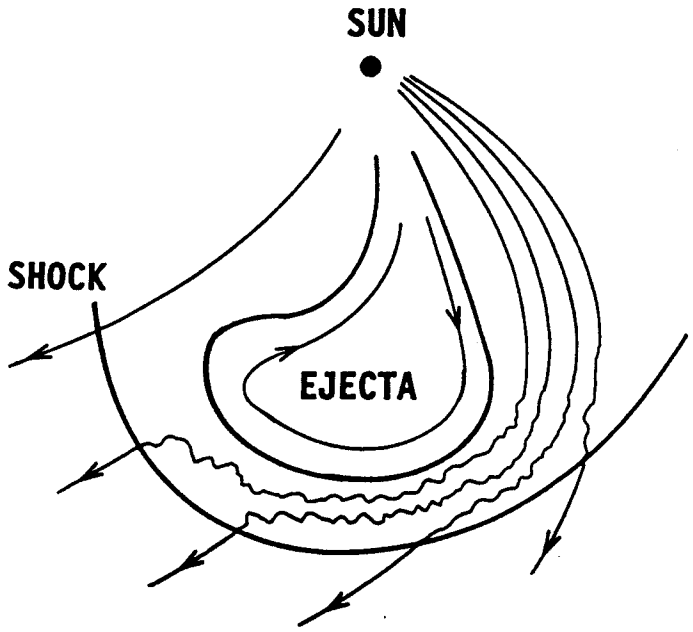

Fig 7

Neugebauer + von Steiger

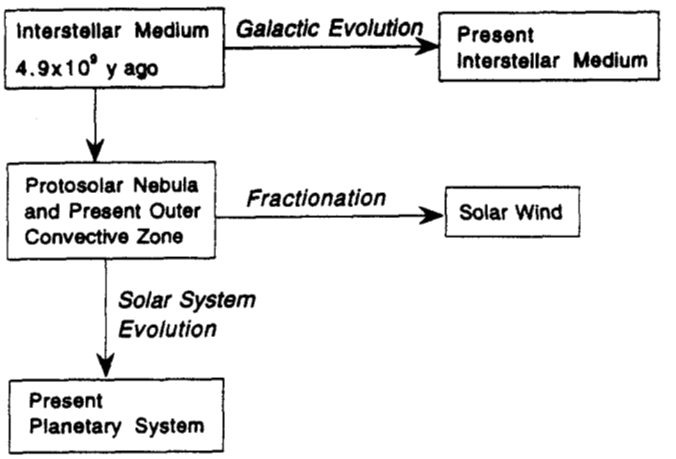

Fig 8

Naugebauer & von Steiger

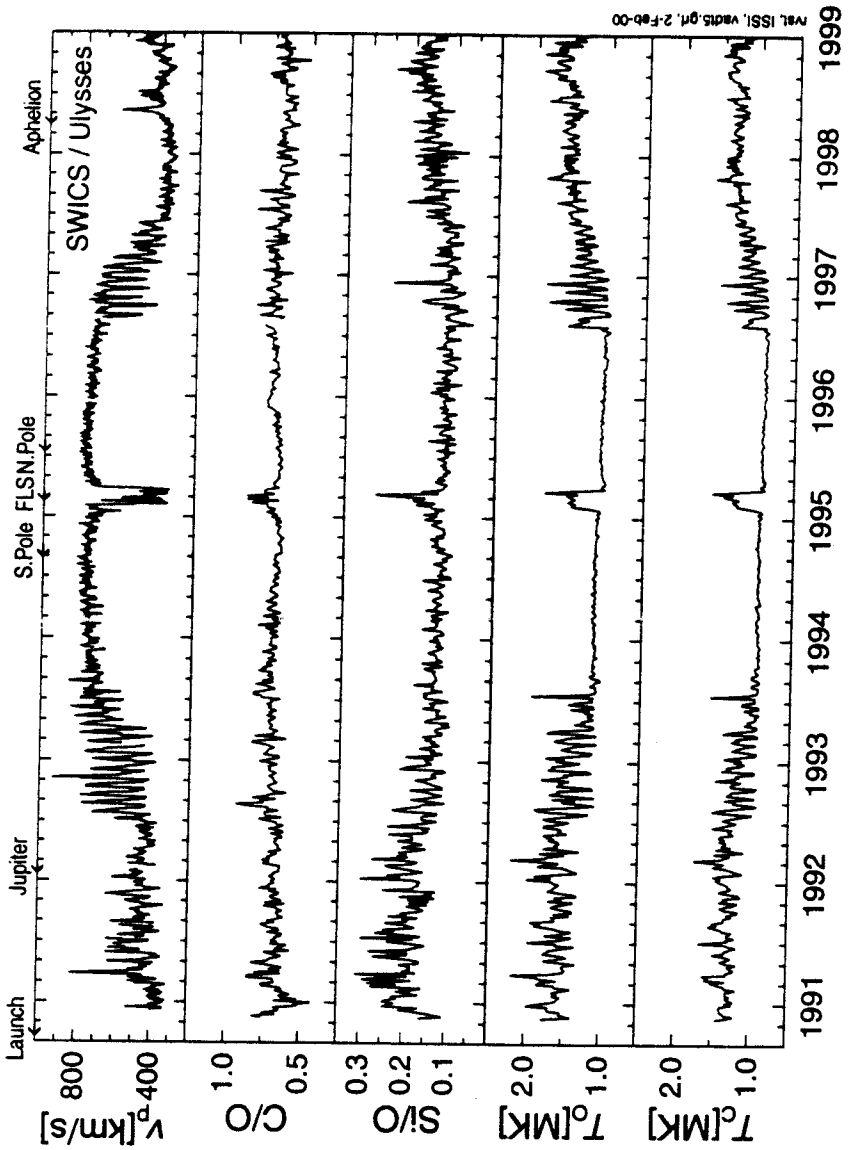

Fig 9

Neugebauer
Vim Steven

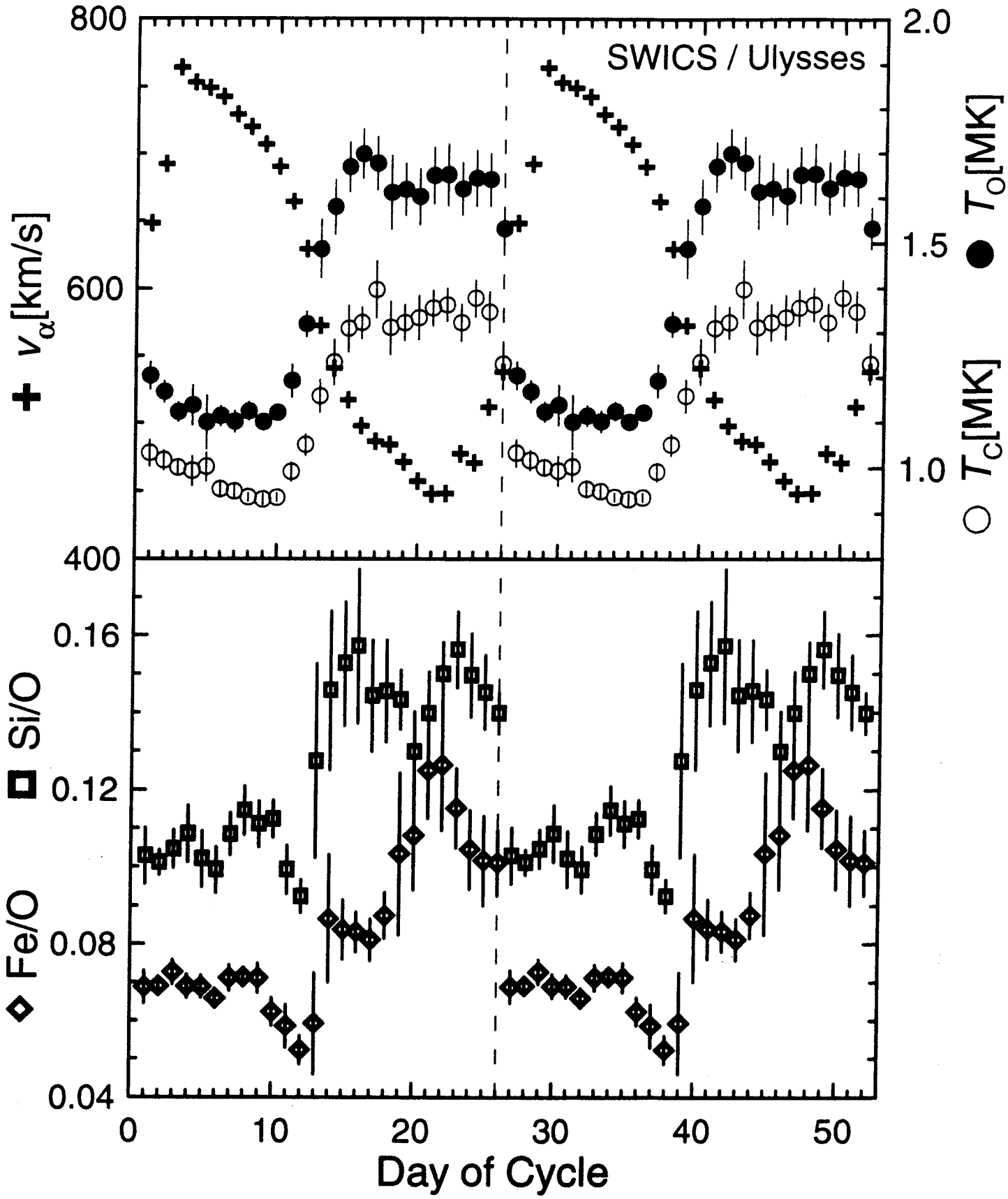

Fig 10
Neugebauer & von Steiger

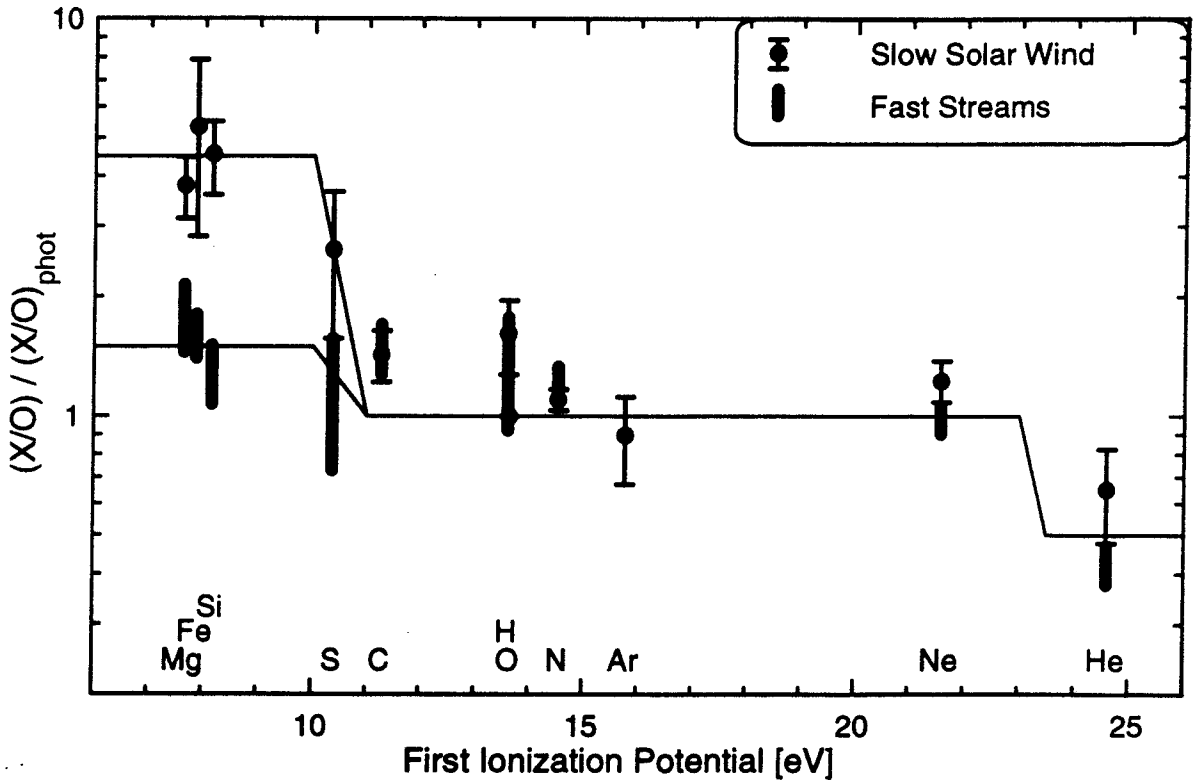

Fig 11

Naughton + von Steiger

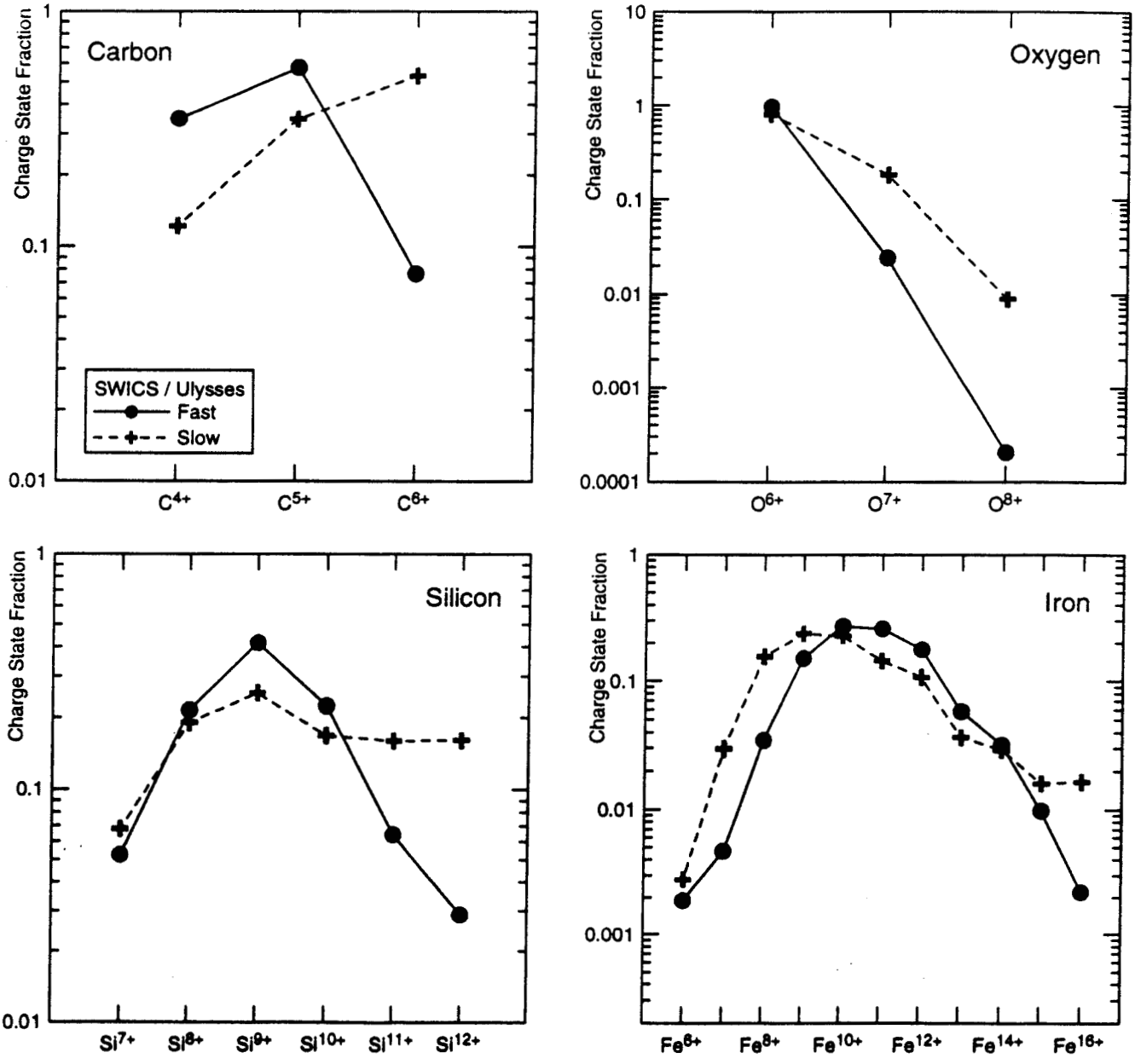

Fig 12

Neugebauer + Von Steiger

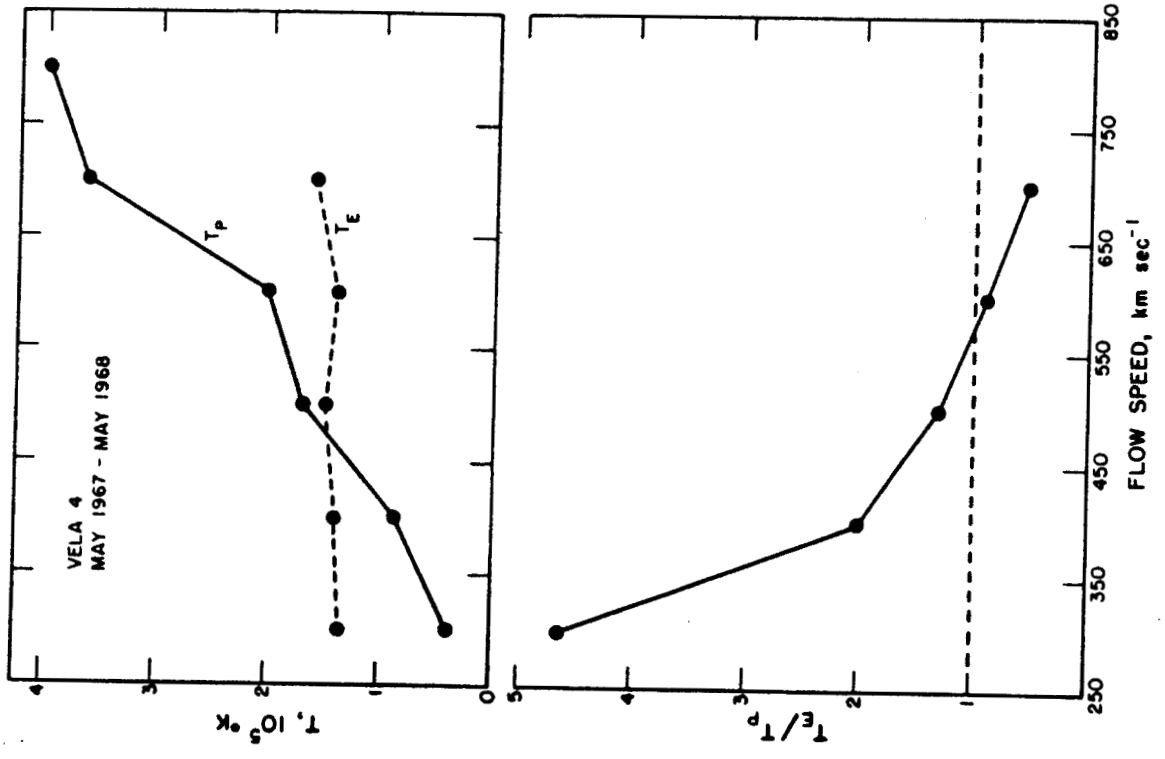

Fig 13

Neugebauer / von Steiger

Fig 14

Neugebauer Steiger

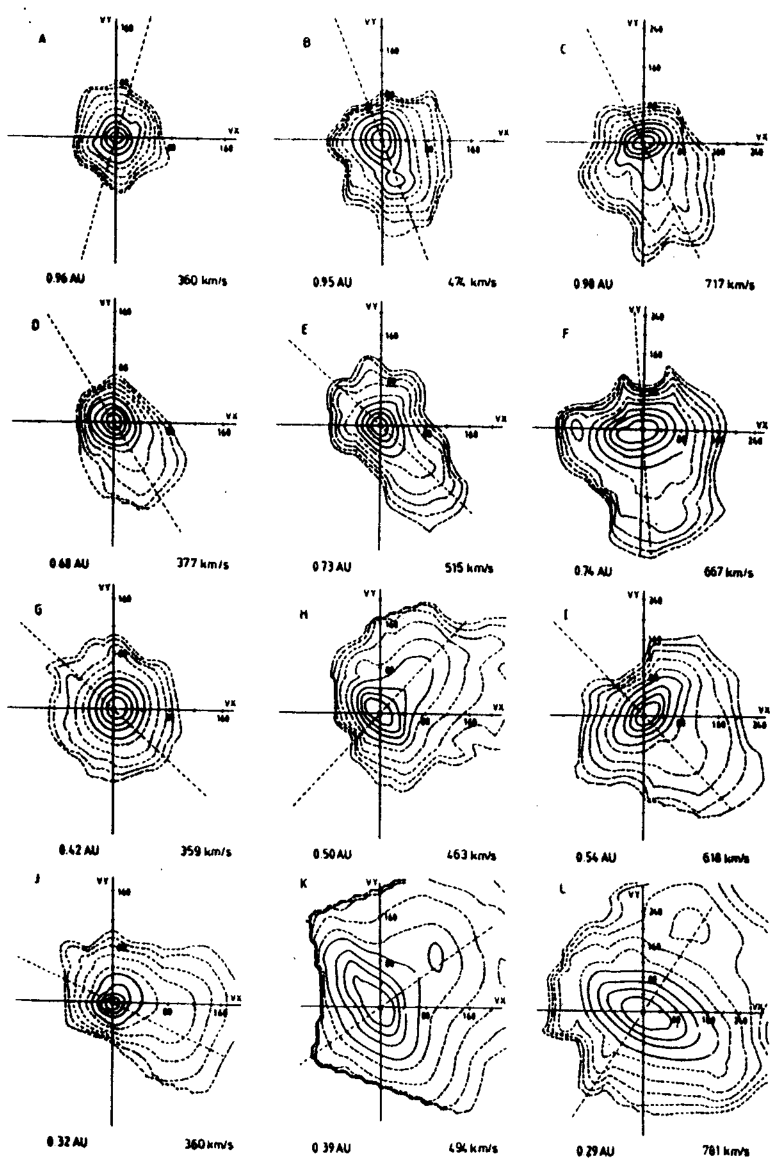

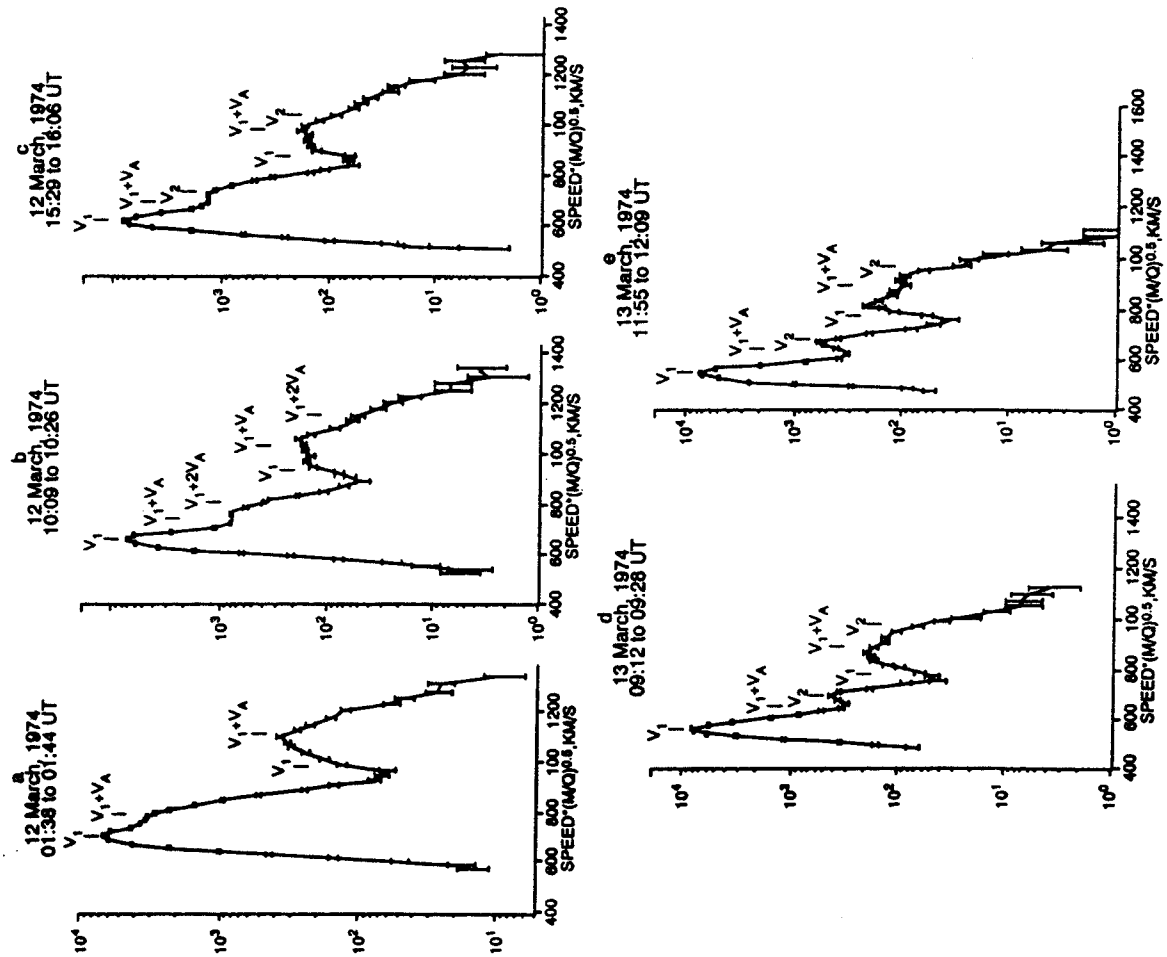

Fig 15

Neugebauer & von Steiger

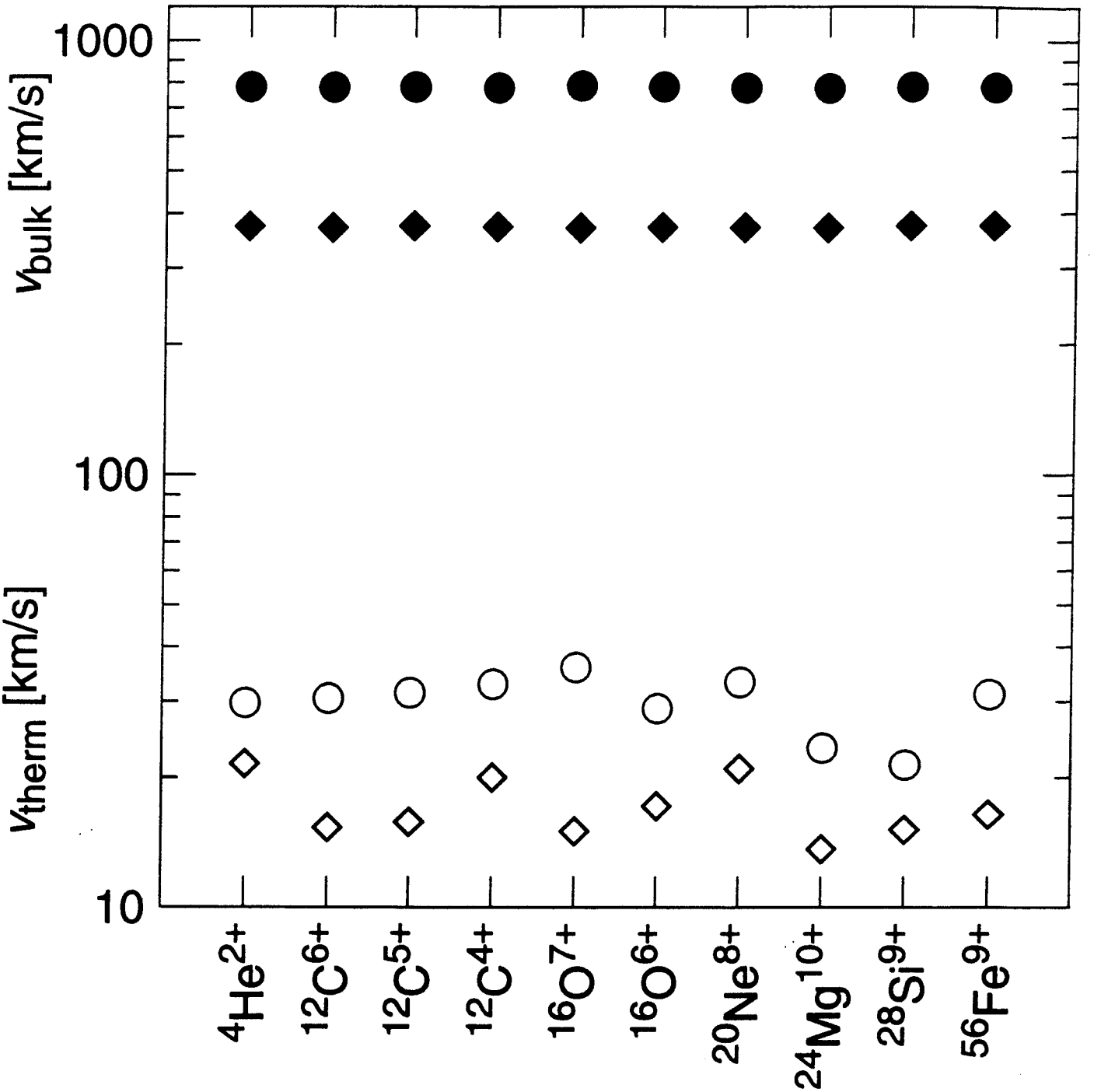

Fig 16

Neugebauer + conStages

Fig. 2.17

Neugebauer + Von Steiger

Fig 18

Neugebauer and Snyder